Renewable and Sustainable Energy Reviews 15 (2011) 1893–1917

Contents lists available at ScienceDirect

Renewable and Sustainable Energy Reviews

journal homepage: www.elsevier.com/locate/rser

Mathematical modeling of solid oxide fuel cells: A review

S. Ahmad Hajimolana[a], M. Azlan Hussain[a,*], W.M. Ashri Wan Daud[a], M. Soroush[b], A. Shamiri[a]

[a] Department of Chemical Engineering, University of Malaya, 50603 Kuala Lumpur, Malaysia
[b] Department of Chemical and Biological Engineering, Drexel University, Philadelphia, PA 19104, USA

ARTICLE INFO

Article history:
Received 23 November 2010
Accepted 27 December 2010

Keywords:
Solid oxide fuel cell
Mathematical modeling
Dynamics
Heat transfer
Mass transfer
Electrochemistry
Polarization
Novel SOFC models

ABSTRACT

This paper presents a review of studies on mathematical modeling of solid oxide fuel cells (SOFCs) with respect to the tubular and planar configurations. In this work, both configurations are divided into five subsystems and the factors such as mass/energy/momentum transfer, diffusion through porous media, electrochemical reactions with and without CO oxidation, shift and reforming reactions, and polarization losses inside the subsystems are discussed. Using variety of fuels fed to SOFCs is issued and their effect on the system is compared briefly. A short review of solid oxide fuel cell configurations and different flow manifolding are also presented in this study. Novel models based on statistical data-driven approach existing in the literatures are considered shortly. Although many studies on solid oxide fuel cells modeling have been done, still more research needs to be done to improve the models in order to predict the fuel cell behaviors more accurately. At the end of this paper the works and studies that can be done for improving the fuel cell models is suggested and pointed by the authors.

Contents

* Corresponding author. Tel.: +60 193706073.
E-mail address: mohd_azlan@um.edu.my (M.A. Hussain).

1364-0321/$ – see front matter
doi:10.1016/j.rser.2010.12.011

1. Introduction

Ever increasing energy consumption, rising public awareness for environmental protection and higher prices of fossil fuels have motivated many to look for alternative/renewable energy sources. Fossil fuel resources are limited and are expected to end early in the next century. By 2015, the world fossil fluid fuel demand will exceed the world fossil fluid fuel production, which is expected to lead to an energy shortage crisis unless a sustainable alternative fuel will be available by them [1–3].

Small-scale power-generation systems such as wind turbines, photovoltaics, micro-turbines and fuel cells can play an important role in meeting consumer demands for "greener" energy. These small-scale generation systems, usually located near customers rather than at central or remote locations, can be used to form distributed power generation networks. Among different types of small-scale power generation systems, fuel cells have received more attention, because they can provide both heat and power. Household fuel cell lets households to generate part of the electricity they require, reducing the electricity purchase from an electric power company. In addition, they serve as a cogeneration system, which use thermal energy produced by electricity generation for water and air heating. It would be best if exhaust heat emitted during the generation process from large-scale power stations could also be converted to thermal energy for heating air or water to use the inputted energy more efficiently. However, it is not considered practical to send hot water (thermal energy) to homes by pipelines from far-removed locations of such large-scale power stations.

Fuel cells are static energy conversion devices that partially convert the chemical energy of fuels directly into electrical energy and produces water as its byproduct [4,5]. The basic principle of the fuel cell was discovered in the year 1838 by Swiss scientist Christian Friedrich Schnbein. In 1839 Sir William Grove developed the first fuel cell based on reversing the electrolysis of water by an accident [3]. In 1950 Francis Bacon at Cambridge University demonstrated the first 5 kW alkalinahoe fuel cell. After the successful development of alkaline fuel cells, NASA needed a compact system to generate electricity for space shuttle applications. In 1970s, international fuel cells developed a 12 kW alkaline fuel cell for NASA's space shuttle orbiter to supply reliable power without the use of any backup powers like batteries. Beginning in the mid-1960s, the research work was focused on further development of various fuel cells for applications like stationary powers and transportations. Further the government agencies in the USA, Canada, Japan and Malaysia have significantly increased their funding for fuel cell in R&D [6].

There are six main types of fuel cell: alkaline fuel cell (AFC), phosphoric acid fuel cell (PAFC), molten carbonate fuel cell (MCFC), polymer electrolyte membrane fuel cell (PEMFC) and direct methanol fuel cell (DMFC), solid oxide fuel cell (SOFC). Table 1 depicts their characteristics briefly.

After the development of power conversion devices, much more researches are doing on solid oxide fuel cells to reduce its higher installation cost. Solid oxide fuel cells are considered to be one of the most advanced designs for mid- to large-scale applications. They are among the most promising types of fuel cells currently being considered as a power source for automobiles and stationary power plants [2,3,7]. Because the electrolyte is a layer of ceramic material with high-temperature endurable porous-media electrodes, SOFCs can generally operate in a high-temperature range (800–1000 C). High operating temperature has some advantages, such as high energy conversion efficiency, flexibility of usable fuel type, and high temperature exhaust gas. Disadvantages include potential thermal fatigue failure of the cell material and sealing under the high temperature, as well as the fact that cell temperature fluctuations induce thermal stress in the cell ceramics. Thus, it is important to operate SOFCs in such a way that the stack temperature remains within a tight design range.

In this case, modeling is a low cost method for studying and investigating the fuel cell in order to optimize and control the fuel cell behavior, increase its efficiency and performance, and finally decrease the higher installation cost. Among many mathematical modeling studies, there are some review papers, concerning different aspects of solid oxide fuel cells investigation which introduce a complete view of all the proceeding works to the researchers who are going to develop and improve them. In this regard, Badwal et al. [8] reviewed the different kinds of materials used in electrolyte and electrodes. Similar work has been done by Zhu et al. [9], presented a review paper about anode materials used in SOFCs. The criteria for the anode of SOFC were first discussed. They also discussed about the problems existing in the developed anode materials. In this paper the advantages and disadvantages of anodes materials were illustrated in order to give a view for further research and development of new generation of anode materials for SOFC. A. Stambouli [6] reconsidered SOFCs as environmentally clean and an efficient source of energy. The advantages and disadvantages of models regarding to AC impedance was studied completely with Q. Huang et al. [10]. Zhang et al. [11] performed a literature study about different strategies and concepts for SOFC-based integration systems, which are timely transformational energy-related technologies available to overcome the threats posed by climate change and energy security. A complete review paper about dynamic models of single-cell SOFCs with respect to various methods, assumptions and models in design, diagnosis and SOFC operation was presented by Bhattacharyya et al. [12] but it was less discussion on steady-state models. The impact of the cell geometry was also presented in their review paper. S. Kakaç et al. [13] reconsidered the numerical models of SOFCs and summarized the present status of the SOFC modeling. V. Lawlor et al. [14] discussed in two parts of a review paper about micro-tubular (MT-SOFC) solid oxide fuel cell. Part I illustrated the reader to the MT-SOFC stack and its applications, indicating who is researching what in this field and also specifically investigate the design issues related to multi-cell reactor systems called stacks. Part II [15] reviewed in detail the combinations of materials and methods used to produce the electrodes and electrolytes of MT-SOFC's. Also the role of modeling and validation techniques used in the design and improvement of the electrodes and electrolytes was investigated. M. Andersson et al. [16] presented a literature study with respect to various transport processes such as mass, heat, momentum, and also charge, electrochemical, shift and internal reforming reactions. This work focused on SOFCs designing by combining the accuracy at microscale with the calculation speed at macroscale, based on clear understanding of transport phenomena,

Table 1
Types of fuel cell [1].

Fuel cell	Temperature (°C)	Efficiency (%)	Application	Advantage	Disadvantages
Alkaline fuel cell (AFC)	50–90	50–70	Space application	High efficiency	Intolerant to CO_2 in impure H_2 and air, corrosion, expensive
Phosphoric acid fuel cell (PAFC)	175–220	40–45	Stand-alone & combined heat & power	Tolerant to impure H_2	Low power density, corrosion & sulfur poisoning
Molten carbonate fuel cell (MCFC)	600–650	50–60	Central, stand-alone & combined heat & power	High efficiency	Electrolyte instability, corrosion & sulfur poisoning
Solid oxide fuel cell (SOFC)	800–1000	50–60	Central, stand-alone & combined heat & power	High efficiency & direct fossil fuel	High temperature, thermal stress failure, coking & sulfur poisoning
Polymer electrolyte membrane fuel cell (PEMFC)	60–100	40–50	Vehicle	High power density, low temperature	Intolerant to CO in impure H_2 and expensive
Direct methanol fuel cell (DMFC)	50–120	25–40		No reforming, high power density & low temperature	Low efficiency, methanol crossover & poisonous byproduct

chemical reactions and functional requirements. Useful methods were investigated for SOFCs modeling. Coupling methods between different approaches and length scales by multiscale models were outlined in order to enhance the understanding for detailed transport phenomena and making a correct decision on the specific design and control of operating conditions. It was remarked that the connection between numerical modeling and experiments is too rare and also that material parameters in most cases are valid only for standard materials and not for the actual SOFC component microstructures.

A review study on mathematical modeling based on steady-state and dynamic behavior, and control of polyelectrolyte membrane and SOFCs with respect to zero- one-, two-, and three-dimensional models was performed by M. Bavarian et al. [17]. The behavior of the fuel cell and processes that occur inside the fuel cells and contribute the existence of multiple time-scales in the fuel cells were investigated and also important components of these models were remarked. It was discussed that under which situations a fuel cell observes steady state multiplicity and also stability of the steady state was issued. In continue, a review of control configurations and strategies by mentioning the advantages and disadvantages of each was presented. Finally, the topics that require further research studies are discussed.

In this study, mathematical modeling of solid oxide fuel cells with respect to the tubular and planar configurations is reviewed into five subsystems considering the factors such as polarization losses, mass/energy/momentum conservations, diffusion through porous media, electrochemical phenomena in the PEN region and shift/reforming reactions inside them which is novel in this regard. Also, using variety of fuels fed to the SOFCs is discussed and their effect on the system is compared briefly. A short review of solid oxide fuel cell configurations and different flow manifolding are also presented in this study. For the first time in this area, novel models based on statistical data-driven approach existing in the literatures are studied. At the end of the paper, it is suggested and pointed which topics need more study for improving the fuel cell models.

The remaining part of this article is organized as follows: Section 2 presents general principle of solid oxide fuel cell; Section 3 discusses mathematical modeling of SOFCs, Section 4 addresses literature on the SOFC configuration; and Conclusion is presented in Section 5.

2. General principle of solid oxide fuel cell

A solid oxide fuel cell uses a hard ceramic electrolyte and operates at temperatures up to 1000 °C. A mixture of zirconium oxide and calcium oxide forms a crystal lattice, although other oxide combinations have also been used as electrolytes. The crystal lattice allows oxide ions to pass through it to reach the anode surface, where the oxide ions combine with H+ ions and form water. The solid electrolyte is coated on both sides with specialized porous electrode materials. The anode consists of a metallic nickel- and Y_2O_3-stabilized ZrO_2 skeleton, which inhibits sintering of the metal particles and provides a thermal expansion coefficient comparable to those of the other cell materials, thus limiting the buildup of stresses resulting from a difference in the coefficient of thermal expansion. The anode structure has a porosity of 20–40% to facilitate mass transport of the reactant and product gases. The cathode material mostly used is strontium-doped lanthanum magnetite ($La_{1-x}Sr_xMnO_3$, for x 0.10–0.15); its structure, such as that of the anode, is porous to permit rapid mass transport of the reactant and product gases. The cathode material has low levels of chemical reactivity with the electrolyte, which extends the lifetime of the material. However, it is a poor ionic conductor, so the electrochemically active reactions are limited to the triple-phase boundary (TPB), where the electrolyte, gas, and electrode meet. In other words, the TPB of a fuel cell is the area of contact between the three phases necessary for electrochemical (hydrogen oxidation and oxygen reduction) reactions at the electrode: an ion-conducting phase, an electron conducting phase, and a gas phase [18]. The bigger the TPB area of a cell, the better the quality of the cell; a bigger TPB area allows the reactions to occur in more sites, thus maximizing current flow. Lanthanum strontium magnetite also works well as a cathode at high temperatures, but its performance quickly decreases as operating temperature decreases to less than 80 °C. The electrochemical reaction occurs when both fuel and air are allowed to flow into the SOFC fuel cell separately. They diffuse through the porous electrode structure to the interlayer and are adsorbed. At the cathode interlayer, oxygen is reduced by the incoming electrons to produce oxygen anions that are conducted through the electrolyte to the anode interlayer where they electrochemically combine with the adsorbed hydrogen to form water and release electrons to the external circuit.

The main advantages of the SOFC is that they can be operated at high efficiency of 50–60% and a separate reformer is not required to extract hydrogen from the fuel due to its internal reforming capability. Waste heat can be recycled to make additional electricity by cogeneration operation [19,20]. The slow start up, high cost and intolerant to sulfur content of the fuel cell are some of its drawbacks. It is not suitable for larger fluctuations in load demand. Therefore, the SOFC is mainly used for medium and large power applications. In 1997 the Ceramic Fuel Cells Limited Company was demonstrated a 5 kW laboratory prototype fuel cell system. Yakabe et al. [21] developed a 3 kW SOFC at Tokyo gas Co. Ltd. And they also analyzed the key factors to improve the performance of SOFC

Table 2
The advantages and disadvantages of PSOFC and TSOFC.

Type of SOFC	Advantages	Disadvantages
PSOFC	-Has the potential to offer higher power density than the tubular design.	-The problems associated with the development and commercialization of planar SOFCs is requirement of high temperature gas seals.
	- Due to its compactness, it can be stacked in resemblance to polymer electrolyte membrane (PEM) fuel cells to satisfy the power requirement of an application.	- Internal stresses in cell components due to non-uniform temperature distributions and high manufacturing cost.
	- Planar SOFC is simple to fabricate and can be manufactured into various configurations.	
TSOFC	- Show great promise as potential candidates to replace conventional heat engines.	-Lower power density than the PSOFC design.
	-Have higher energy efficiency.	- Have high ohmic loss
	- They are designed for mid- to large-scale applications up to 2 MW.	

in the micro-grid system and are building a 250 kW commercial stack model.

2.1. SOFC configurations

There are two principal SOFC configurations, tubular and planar. The Schematic of tubular and planar SOFC is illustrated in Figs. 1 and 2 respectively. Tubular configuration consists of two tubes, an outer tube and an inner tube. The outer tube is the cell tube. The outer surface of the cell tube is anode side of the cell, and its inner surface is the cathode side. Between the anode and cathode sides lies the solid oxide electrolyte. The inner tube is an air injection and guidance tube, composed of alumina, from which preheated air is injected into the bottom of cell tube and flows over the cathode surface of the cell tube through the gap between the injection and cell tubes. The end of the cell tube is closed. Fuel gas flows over the anode surface through the gap among the cell tubes. Oxygen ions pass through the cathode and electrolyte and react with fuel, creating an electric current. A major advantage of tubular Solid Oxide Fuel Cells (TSOFCs) over other types of fuel cells is that a variety of hydrocarbon-based gases or their synthesis derivatives, such as natural gas, biomass and coal can be potentially used as fuel sources. CO present in the synthesis gas can be oxidized in TSOFCs to generate CO_2 and electrical energy. The disadvantage of tubular SOFC compared to planar SOFC is that the ohmic losses are much higher due to the longer ways of electrical current.

Generally, planar configuration is constructed of a positive-electrolyte-negative electrode (PEN), interconnect top and bottom of the cell stack, air and fuel channels. The fuel gas channel is between the anode and the separator plate and on the other side the air channel is located between the cathode and separator plate. Recognizing the advantages of the low-cost, simplicity in manufacturing and high volume manufacturing with high volumetric power densities, most fuel cells manufacturers are concentrating on the planar SOFC concept. However, a challenge with the planar geometries is in obtaining mechanically stable structure, as thin layer ceramics are inherently susceptible to failure when subjected to moderate stresses. The planar concept provides the largest area for the current collector but it shows disadvantages in start-up time and mechanical stability. The advantages and disadvantages of two types of SOFC are depicted in Table 2.

Based on the thicknesses of the electrodes and electrolyte layers, SOFCs are divided also into three types namely anode-supported, electrolyte-supported and cathode-supported. It was explored that ohmic and polarization losses in electrode-supported are smaller than in electrolyte-supported cells [22].However, the anodic polarization is smaller than the cathodic one [23]. Moreover, anode-supported solid-oxide fuel-cells can operate at lower temperatures, which results in diminished manufacturing costs [24]. For these reason anode-supported cells are often considered to be the preferred configuration for SOFCs. But the thick anode

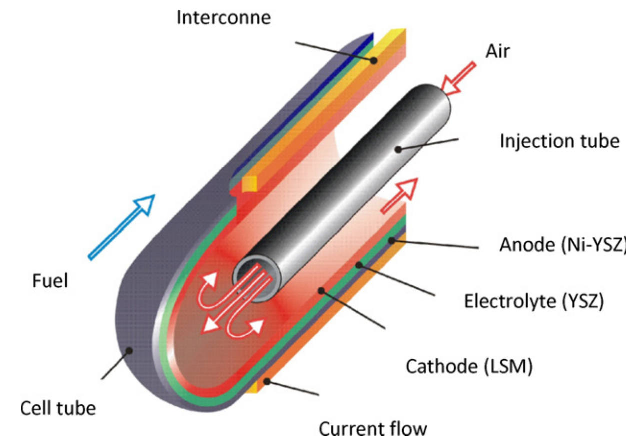


Fig. 1. Schematic of tubular SOFC.

supported structure leads to enhance the concentration polarization due to diffusion limitation, and thus decreases the fuel cell performance [25].

Regarding the flow configuration, there are three main types flow inside the fuel cells namely co-flow, counter-flow and cross-flow.

3. Mathematical modeling of solid oxide fuel cells

Mathematical modeling is an essential tool in designing fuel cell systems which represents the important aspects of the existing system and presents knowledge of that system in usable form. In other word, such models can provide a picture of voltage, current density, temperature, velocity and concentration of components as functions of position and time for various cell configurations and operating conditions. The effect of different variables and their sensitivity on the fuel cell performance can be studied by these mathematical models. A model is also useful in predicting the effects of altering process variables and in using that information to optimize cell performance. Moreover, dynamic simulation can provide reference for the control system research and design in future.

Solid oxide fuel cell modeling for both the tubular and planar configurations tacked into account the electrochemical model, diffusion through porous media, the mass, energy, and momentum conservation balances.

To perform first-principles model of the SOFC for the both configurations, single tubular and planar fuel cells are considered and divided into several subsystems as shown in Figs. 3 and 4.

For the tubular SOFC the subsystems are as follow:

- Subsystem 1 (SS1): air inside the injection tube;
- Subsystem 2 (SS2): injection tube;

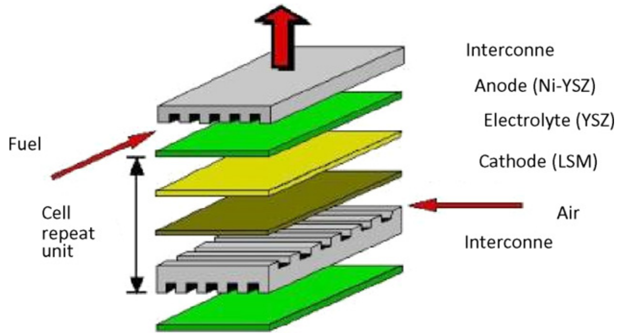


Fig. 2. Schematic of planar SOFC.

- Subsystem 3 (SS3): air inside the space between the cell and injection tubes;
- Subsystem 4 (SS4): cell tube;
- Subsystem 5 (SS5): fuel mixture over the anode side of the cell tube.

For the planar SOFC the subsystems are as follow:

- Subsystem 1 (SS1): air channel;
- Subsystem 2 (SS2): air side interconnector;
- Subsystem 3 (SS3): fuel side interconnector;
- Subsystem 4 (SS4): cell tube;
- Subsystem 5 (SS5): fuel channel.

The SOFCs models are then derived by writing the appropriate electrochemical and transfer phenomena equations.

3.1. Model equations for subsystem 1 (SS1)

This subsystem for TSOFC includes the air inside the injection tube and for PSOFC is the air flow inside the air channel, between air side interconnector and cathode. In this subsystem, mass/energy/momentum transfer models can be accounted.

3.1.1. Mass transfer model

Gas transport is important to enhance the performance of the fuel cell. The performance of a SOFC at high operating current densities is reduced mainly due to the mass transport losses. Micro-structural parameters also largely affect the gas transport. Mass transport models inside the electrodes are giving an accurate prediction for gas concentration at the anode-electrolyte-cathode interface. Therefore; an accurate modeling of this phenomenon is imperative for development of better fuel cell designs.

(i) A mass balance on the air inside SS1 for TSOFC takes the form

$$\frac{\partial \rho_{air}^{inj}}{\partial t} + \nabla(u^{inj}\rho_{air}^{inj}) = 0 \quad (1)$$

(ii) A mass balance on the air and O_2 inside SS1 (cathode channel) for PSOFC takes as the follow:

$$\frac{\partial \rho_{air}^{ch,c}}{\partial t} + \nabla(u_{air}^{ch,c}\rho_{air}^{ch,c}) = -\nabla N_{O_2} \quad (2)$$

$$\frac{\partial \rho_{air}^{ch,c} Y_{O_2}}{\partial t} + \nabla(u_{air}^{ch,c}\rho_{air}^{ch,c} Y_{O_2}) = -\nabla N_{O_2} \quad (3)$$

where i denotes the generic i_{th} specie, Y_{O_2} the mass fraction of the O_2 species, ρ is the density, u is the gas velocity and ∇N_{O_2} is the diffusion of O_2 into the porous cathode for participating in electrochemical reaction, Superscripts *inj* and *ch,c* denote injection tube and cathode channel, respectively.

Although mass transfer via diffusion inside the fuel cell significantly affects the fuel cell performance, some researchers like Costamagna et al. [26], Burt et al. [27], Stiller et al., [28], Ji et al. [29] neglected diffusion of components through media electrodes. Burt et al. [27] were assumed that changes in the *x*-direction are small and can safety be ignored.

The diffusion through the porous media was modeled by writing detailed mass transfer equations with many researchers like Chan et al. [30], Yakabe et al. [31], Bove et al. [32], Ho et al. [33], Qi et al. [34] and others [35–41]. In these works, it was observed that the fuel cell behavior was more accurately than the models neglected the diffusion of gases in the electrodes.

The diffusion of component through porous electrodes is assumed by using one of the three approaches as the following:

(a) Fick's Law model (FLM) is the simplest diffusion model and used in dilute or binary systems by Stiller et al. [28], Chan et al. [30], Bove et al. [32], Hussain et al. [37] and many other researchers [30,32,37–40,42–53]. The model is given by:

$$N_i = [D_i \nabla(\rho Y_i)] \quad (4)$$

where D_i is the diffusion coefficient.

(b) The Stefan–Maxwell model (SMM) is more commonly used in multi-component systems for calculation of specie fluxes. The model is given by:

$$-\nabla(Y_i) = \sum_{j=1,j\neq i}^{n} \frac{Y_i N_i - Y_i N_j}{CD_{i,j}} \quad (5)$$

where N is the species flux and C is the concentration.

Some other researchers like Bhattacharyya et al. [54], Virkar et al. [55] Kim et al. [56] Bove et al. [57], Sánchez et al. [58,59] and Jin et al. [60] considered SMM model in their survey.

(c) The Dusty Gas model (DGM), is the extended model of Stefan–Maxwell equation, which is the most complete diffusion model considering molecule-molecule and molecule-wall interactions in the porous media, commonly used as well, because it takes into account Knudsen diffusion phenomena and neglect the assumption of equal-molar counter diffusion in Fick's law, which becomes invalid if the molecular weights of the diffusing gas species differ widely. The model is given by:

$$-\nabla(Y_i) = \frac{N_i}{D_{i,k}} + \sum_{j=1,j\neq i}^{n} \frac{Y_i N_i - Y_i N_j}{CD_{i,j}} \quad (6)$$

In many surveys this model is used [38,49,61–71]. Tseronis et al. [72] and Cayan et al. [40] used a combination of diffusion method.

Tseronis et al. [72] discussed multidimensional model transport phenomena in an anode channel and diffusion through porous anode in an isothermal planer SOFC based on a combination of the Stefan-Maxwell and Dusty gas method. The results were validated with experimental data (Yakabe et al. [31]).

Cayan et al. [40] illustrated a two-dimensional model based on mass transfer inside an SOFC. In this survey, diffusion methods, Stefan-Maxwell and Fick's law relations, both including Knudsen diffusion, in order to predict the species concentration gradient was compared. The results showed that at low current densities, both models are well in agreement while by increasing the current the differences becomes bigger.

A complete survey for performance comparison of Fick's model, dusty gas model and Stephan-Maxwell model have been done by R. Suwanwarangkul et al. [52]. It was showed that DGM is the most suitable model for the H_2-H_2O and CO-CO_2 systems due to the Knudson diffusion impact. However, due to its complexity, this

model can only be used at the conditions of low reactant concentration, high operating current density and small pore size where high accuracy of model prediction is needed. Otherwise, the SMM is a useful model for H_2-H_2O system and FM is suitable for the CO-CO_2 system. SMM does not tacked into account the Knudson diffusion term in order to calculate the pore size effect while both FM and DGM do. It was fund that the equimolar counter diffusion is assumed to determine the flux ratio in both FM and the SMM. By contrast, the flux ratio in the DGM is calculated from the ratio of the square-root of the gas molecular weight. It was illustrated that DGM is suitable for multi-component system of H_2–H_2O–CO–CO_2, because the flux ratio calculation is complicated and equimolar counter diffusion cannot be assumed. Moreover, the Knudson diffusion effect must be considered.

Diffusion through the porous material is typically described by either ordinary or Knudsen diffusion and has been found to play an important role in catalytic reaction. Ordinary diffusion occurs when the pore diameter of the material is large in comparison to the mean free path of the gas molecules. Molecular transport through pores which are small in comparison to the mean free path of the gas is regarded as a Knudsen type of diffusion. For Knudsen diffusion, molecules collide more frequently with the pore walls than with other molecules. Upon collision, the atoms are instantly adsorbed on to the surface and are then desorbed in a diffusive manner. As a result of frequent collisions with the wall of the pore, the transport of the molecule is impeded. The Knudsen diffusion coefficient can be predicted using kinetic theory by relating the diameter of the pore and the mean free path of the gas. For straight and round pores, the diffusion coefficient is given by [30]:

$$D_{Ak} = 97.0\vec{r}\sqrt{\frac{T_{ct}}{M_A}} \tag{7}$$

where T_{ct} is the cell tube temperature, and $\vec{r}$ is mean pore radius which can be calculated from the bulk density, S_A area of the porous solid, and ε porosity [30].

$$\vec{r} = \frac{2\varepsilon}{S_A \rho_B} \tag{8}$$

To account for the tortuous path of the molecule rather than along the radial direction and the porosity of the solid electrode for the fact that diffusion occurs only in the pore space, an effective Knudsen diffusion coefficient may be used, i.e. [30]:

$$D_{Ak(eff)} = D_{Ak}\left(\frac{\varepsilon}{\zeta}\right) \tag{9}$$

where ζ is the tortuasity.

Using the Chapman-Enskog theory of prediction, the binary ordinary diffusion coefficient in the gas phase [73] can be calculated as follows which was used by Yakabe et al. [21], Chan et al. [30], Ni et al. [41] and many other researchers [21,30,39–41,45,46,54,74–76].

$$D_{AB} = 0.0018583\left(\frac{1}{M_A} + \frac{1}{M_B}\right)^{1/2} \frac{T^{3/2}}{P\sigma_{AB}^2 \Omega_{DAB}} \tag{10}$$

where p is the total pressure, $\sigma_{AB} = (\sigma_A + \sigma_B)/2$ is the collision diameter and Ω_{DAB} is the collision integral based on the Lennard-Jones potential which can be obtained from e_{AB} is the energy of molecular interaction:

$$\frac{e_{AB}}{k} = \sqrt{\left(\frac{e_A}{k}\right)\left(\frac{e_B}{k}\right)}. \tag{11}$$

Neufield et al. [73] is given by:

$$\Omega_D = \frac{1.06036}{(kT/\varepsilon_{AB})^{0.15610}} + \frac{0.19300}{\exp(0.47635(kT/\varepsilon_{AB}))} + \frac{1.03587}{\exp(1.52996(kT/\varepsilon_{AB}))} + \frac{1.76474}{\exp(3.89411(kT/\varepsilon_{AB}))} \tag{12}$$

Hajimolana and Soroush [22], Qi et al. [34], Bhattacharyya et al. [54] and other authors [22,34,53,54,59,64,77–79] used Fuller et al. correlation which is given by [80]:

$$D_{ij} = \frac{1.013 \times 10^{-7} T_{ct}^{1.75}[(1/M_{O_2}) + (1/M_{N_2})]^{1/2}}{[P_{O_2}^{TPB} + P_{air}^{cat}(1 - \zeta_{O_2}^{cat})](kT/\varepsilon_{AB})^2} \tag{13}$$

The effective diffusion coefficient can be written as [80]:

$$\frac{1}{D_{A(eff)}} = \frac{1}{D_{AB(eff)}} + \frac{1}{D_{Ak(eff)}} \tag{14}$$

Chapman and Enskog is the most common method for theoretical estimation of gases penetration in the porous electrodes while Fuller correlation is derived based on the experimental and empirical data [81,82].

Table 3 shows some researchers that focused on mass transfer in their model.

3.1.2. Heat transfer model

In all the models that has been considered the thermal model, showed that the material properties, chemical kinetics, and transport properties of materials used in a single cell and stack depends on the temperature. Therefore, it is essential to develop a heat transfer model that could account for various heat effects in both of the solid structure and the flow channels. However, many researchers assumed an isothermal system in their model [38,60–62,64–66,83–87]. On the other hand, several literatures studied on heat transfer modeling in details in order to show the magnitude of heat transfer components. Fig. 5 shows a comparison between a non-isothermal and isothermal models. This figure depicts the responses of voltage in both isothermal and non-isothermal conditions by changing a fuel cell load. As it can be seen in Fig. 4, at the non-isothermal condition the voltage response is slow in comparison with the isothermal condition, since the heat capacity of solid materials is large and causing a slow response. This figure shows that temperature strikingly affects the fuel cell system and thus it is noteworthy to account energy balance in the SOFCs modeling. Table 4 depicts some authors that focused on heat transfer in their model.

(i) An energy balance for the TSOFC inside the injection tube (SS1) has the form:

$$\frac{\partial \rho_{air}^{inj} H_{air}^{inj}}{\partial t} = \nabla \Delta \rho_{air}^{inj} u_{air}^{inj} H_{air}^{inj} + Q_{conv}^{inj} + Q_{rad}^{inj} \tag{15}$$

This equation represents the transport of energy in the injection tube by bulk fluid flows ($\nabla \Delta \rho_{air}^{inj} u_{air}^{inj} H_{air}^{inj}$), convection heat transfer (Q_{conv}^{inj}) and radiation between air flow components (Q_{rad}^{inj}).

Temperature of the inlet air stream into the SS1 has the strongest effect on the cell performance [22,43].

Convection heat transfer in SS1 for TSOFC is between air flow temperature and inside the wall of injection tube which is given by:

$$Q_{conv}^{inj} = h_{it_i}(T_{it_i} - T_{air}^{inj}) \tag{16}$$

where h is the convection heat transfer coefficient, T_{air}^{inj} is the air flow temperature inside the injection tube. Subscript it_i is inside the of injection tube.

Table 3
Selected studies concerning on mass transfer through the SOFCs.

Author	Cell type	Objective	Method	Short coming	Assumption
Izzo Jr et al. [38]	Micro-TSOFC	- Studying the gas flow through an anode-supported tubular SOFC and the subsequent diffusion of gas through its porous anode.	Gas diffusion was modeled using the dusty-gas equations.	The effect of DGM on fuel cell performance was not compared with FL and SMM.	1D, Steady state, isothermal
		-predict the polarization of the fuel cell	Mercury intrusion porosimetry (MIP) was used to experimentally determine micro-structural parameters.		
Bhattacharyya et al. [76]	TSOFC	-Study the effect of Knudson diffusion	In the process of validation, phenomena that affect the transient response of the cell significantly were identified.	-The effect of Three diffusional models was not considered.	2D diffusion, isothermal dynamic model of an anode-supported tubular counter-flow
		-Study the system response and compare with experimental results.		-Further modifications may be needed in order to have a validated steady state and dynamic model in a broader operating range.	
Hussain et al. [37,83]	Anode-supported SOFC	-Develop a mathematical model to describe the transport of multi-component species inside the porous anode including reaction zone layer.	A modified Stefan–Maxwell equations incorporating Knudsen diffusion were used to model the multi-component diffusion inside the porous anode.	-It was not clear among three diffuisional models why SMM was used in this model.	1D steady state, Isothermal
		-To anticipate the distribution of multi-component species in the electrode and reaction zone layers at different current density by the composition of ethanol reformate fuel.		-The momentum of gaseous species in porous anode was assumed to be negligible.	
		-Study the effect of shift reaction and finite reaction zone layer on the concentration overpotential.		-The effect of viscose and gravity for ideal gases was ignored.	
Lehnert et al. [65]	SOFC	To describe the transport of gases inside the SOFC anode due to diffusion	Mass transport phenomena in the porous cermet, such as diffusion and permeation, accompanied by chemical and electrochemical reactions internal reforming and electrochemistry were studied and the resulting model is implemented in a numerical simulation program.	-It was not validated with experimental data.	1D, isothermal steady state
Suwanwarangkul et al. [52]	TSOFC	To evaluate the various mass transport models by validating them with the measured concentration overpotential data obtained from Yakabe et al. [42].	Three types of models including Ficks' model, the dusty gas model and the Stephan-Maxwell model inside the porous SOFC anode were developed to predict the concentration overpotential.	- The total pressure gradient inside the electrode was assumed to be negligible.	1D steady state, Isothermal

(ii) An energy balance for the PSOFC inside the cathode channel (SS1) has the form:

$$\frac{\partial \rho_{air}^{ch,c} H_{air}^{ch,c}}{\partial t} = \nabla \Delta \rho_{air}^{ch,c} u_{air}^{ch,c} H_{air}^{ch,c} + Q_{conv}^{ch,c} + Q_{rad}^{ch,c} + Q_{diff}^{ch,c} \qquad (17)$$

This equation represents the transport of energy in the cathode channel by bulk fluid flows ($\nabla \Delta \rho_{air}^{inj} u_{air}^{inj} H_{air}^{inj}$), convection heat transfer (Q_{conv}), radiation between air flow components, cathode side interconnector wall and cathode wall (Q_{rad}) and diffusional heat transfer by oxygen (Q_{diff}).

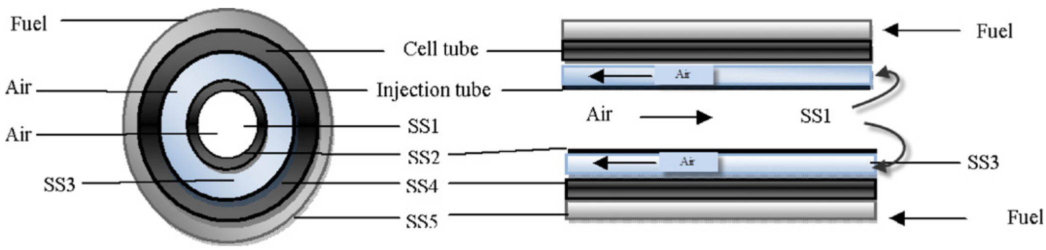


Fig. 3. Division of the single TSOFC into five subsystems.

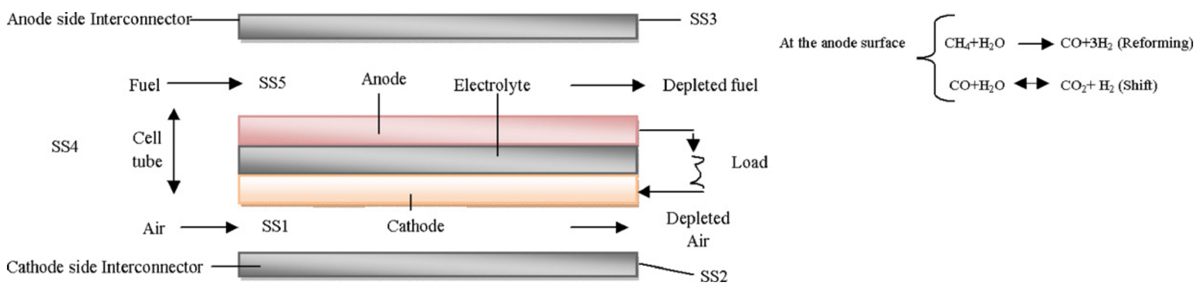


Fig. 4. Division of the single DIR-PSOFC into five subsystems.

Table 4
Selected studies concerning on heat transfer through Solid Oxide fuel.

Author	Cell type	Objective	Method	Short coming	Assumption software
Inui et al. [89]	PSOFC	Numerically optimize the operating parameters of the cell and the temperature of the inlet gas	Concerning the calculation of the gas flow in each channel, the one dimensional steady state mass and energy conservation equations were used, and the flow was determined by integrating these equations from the cell inlet to its outlet.	The radiation heat transfer was not considered	1D transient
Daun et al. [90]	PSOFC	Show the importance of radiation thermal transfer.	Two different radiation solvers were employed to solve for the radiation source term in the electrolyte: the Schuster Schwarzschild two-flux method [138] and a collision-based Monte Carlo method [139].	-The flow properties such as heat capacity, viscosity were not considered, -The enthalpy and entropy were assumed constant and are not a function of temperature -Diffusional heat transfer was not considered	2D steady state
Tanaka et al. [91]	PSOFC	Examine the effect of the heat transfer due to radiation on the cell operation,	It was developed a three dimensional simulation code of the planar SOFC stack	The time dependent calculation was performed only for the cell temperature distribution.	3D steady state
Damm et al. [92]	TSOFC	Understanding, predicting, and quantifying the effects of radiation in SOFC materials and systems.	Modeling surface-to-surface radiative exchange, Radiative transfer in the flow Channels and Heat loss from the edges	Shift/ reforming heating and diffusional heat transfer were neglected.	1D steady state
Brus et al. [93]	TSOFC-IIR	To describe numerical modeling of the radiative heat transfer process	Heat transfer between the fuel reformer surface and all other surfaces facing the reformer surfaces was modeled	-The flow properties such as heat capacity, viscosity were not considered -The enthalpies were assumed to be constant	
Sĭanchez et al. [58]	TSOFC	To simulate a complicated heat transfer model and compare the errors used for those with simple models with the complex model.	The work was divided in two parts. First, two models for describing convective heat transfer was proposed. For the radiation heat transfer, two models were presented again	-The velocity and mass flow were assumed constant along the length therefore the conduction heat transfer coefficient was constant.	1D steady state

Convection heat transfer in SS1 for PSOFC is between air flow and both cathode channel and cathode side interconnector walls which is given by:

$$Q_{conv}^{ch,c} = h_{\text{int},c_i}(T_{\text{int},i}^{cat} - T_{air}) + h_{ct,c_o}(T_{ct,c_o} - T_{air}) \quad (18)$$

where subscripts int,c_i and ct,c_o are inside the cathode side interconnector and outside the cathode side of the cell tube, respectively, and superscript *cat* is the cathode side.

An empirical Nusselt number correlation is used to calculate the convection heat transfer coefficient:

$$NU = f(Re, Pr) \quad (19)$$

$$NU = \frac{h_c D}{K} \quad (20)$$

D is the fuel cell diameter.

By Hayes and Kolaczkowski [88] expression Nusselt number yields as the follow:

$$NU = 3.095 + 8.933\left(\frac{1000}{Gz}\right)^{-0.5386} \exp\left(-\frac{6.7275}{Gz}\right) \quad (21)$$

where the Greatz number Gz is given by

$$Gz = \frac{D}{x} RePr \quad (22)$$

x is the axial position, Re and Pr are the Reynolds number and Prantl number, respectively.

For a fully developed laminar flow approximation at constant wall temperature Nusslet number is assumed to be 3.66.

For $Re > 2300$, $0.5 < \Pr < 2000$ and $L > D_h$ Gienelinski's equation is applicable:

$$NU = \frac{Pr(Re - 1000)(f/8)}{1 + 12.7(Pr^{2/3} - 1)\sqrt{f/8}}\left(1 + \left(\frac{D_h}{L}\right)^{2/3}\right) \quad (23)$$

$$f = (0.79\ \ln(Re) - 1.64)^{-1} \quad (24)$$

where D_h is hydraulic diameter, L the length of fuel cell and f friction factor. However this equation has complexity for calculating the convection coefficient.

Colburn's equations is easier to use but have errors around 20% [58]:

For laminar flow:

$$NU = 0.332 Pr^{1/3} Re^{1/2} \quad (25)$$

For turbulent flow:

$$NU = 0.023 Pr^{1/3} Re^{4/5} \quad (26)$$

In some studies constant values for h and K at transient condition are assumed [83,89]. In the study of D. S'anchez et al. [58] the effect of constant and variable convective heat transfer on fuel cell was compared. The results showed that these two models substantially affect the temperature at both ends of the fuel cell tube while there is no impact on the shape of temperature *curve*. Some authors like Hajimolana and Soroush [22], Ji et al. [29] and Qi et al. [43] calculated thermal conductivity, convection heat transfer coefficient, viscosity, specific heat capacity, enthalpy and specific resistivity as a function of temperature. The values of conduction and convection heat transfer coefficient existing in the literatures are illustrated in Table 5.

Energy transportation inside and outside of the mass media occurs by diffusion of components. Diffusional heat transfer is available in [22,39,41,43,46,48,90–92]. However, this type of heat transfer was not involved in some literatures because it was assumed that it is not magnitude compared to the conduction heat transfer in porous media [61,67].

Table 5
Different values of conduction/convection heat transfer coefficient.

Authors	h_c (kJ/m² s K)	K (kJ/m s K)
Aguiar, P. et al. [95]	$h_{c,a} = hc,c = 0.1$	2×10^{-3}
Damm et al. [92]	$h_{c,a} = hc,c = 0.6$	$K_a = 0.00584$ $K_c = 0.00186$ $K_{elec} = 0.00216$ $K_{air\,channel} = 0.000047$ $K_{fuel\,channel} = 0.0002$
Denver et al. [92]	$h_{c,a} = h_{c,c} = 0.302$	
Xue et al. [84]	$h_{c,a} = 2.987$ $h_{c,c} = 1.322$	$K_a = K_c = K_{elec} = 0.00253$

For PSOFC in SS1, oxygen diffuses into the cathode in order to participate in electrochemical reaction, thus the diffusional heat transfer leads to:

$$Q_{diff}^{ch,c} = \nabla N_{O_2} H_{O_2} \quad (27)$$

Air mainly consists of non-polar nitrogen and oxygen molecules and therefore, is non-interaction (transparent) with radiation heat transfer at the moderate temperatures and pressures within SOFCs [93]. Therefore, no radiation heat transfer occurs between the air properties. So in SS1 for both TSOFC and PSOFC no radiation heat transfer occurs.

3.1.3. Momentum model

Velocity affects the film heat transfer coefficient on the anode and cathode side. An increase in the gas flow velocity leads to an increase in the film heat-transfer coefficient, causing the removal of more energy from the cell tube, resulting in a decrease in the cell-tube temperature [22]. On the other hand, velocity is affected by reactions, mass transfer, density change, etc. The flow velocities can be modeled by the momentum conservation.

(i) A momentum balance inside the TSOFC inside the injection tube (SS1) based on Navier-Stokes equation leads to [94]:

$$\frac{\partial(\rho_{air}^{inj} u_{air}^{inj})}{\partial t} + (\nabla \rho_{air}^{inj} u_{air}^{inj} u_{air}^{inj}) = -\nabla P_{air}^{inj} + \nabla \tau_{air}^{inj} + F_{air}^{inj} \quad (28)$$

where ($\nabla \rho uu$) is the momentum rate flowing in and out of the SS1, ∇P the pressure gradient, τ is the shear stress, and F is prescribed body force (i.e. gravity force).

(ii) A momentum balance for the PSOFC inside the cathode channel (SS1) based on Navier-Stokes equation leads to [94]:

$$\frac{\partial(\rho_{air}^{ch,c} u_{air}^{ch,c})}{\partial t} + (\nabla \rho_{air}^{ch,c} u_{air}^{ch,c} u_{air}^{ch,c}) = -N_{O_2} M_{O_2} u_{air}^{ch,c} - \nabla P_{air}^{ch,c} + \nabla \tau_{air}^{ch,c} + F_{air}^{ch,c} \quad (29)$$

where $N_{O_2} M_{O_2} u$ is the momentum out flow rate resulting from O2 participation in the electrochemical reaction.

Ferguson et al. [50], Janardhanan et al. [67] and other researchers [50,67,78,95–97] neglected the momentum conservation in their model, while many researchers like Hajimolana and Soroush [22], Bove et al. [32], Autissier et al. [35], Qi et al. [43], Suwanwarangkul et al. [51] and others [32,35,39,43,45,51,53,54,61,63,66,69,77,78,83,86,91,98–103] considered the momentum conservation in their model. Bhattacharyya et al. [54] compared the models with and without momentum conservation and found that the change in velocity, especially in the cathode side channel is significant. When momentum conservation is involved in the model the concentration of oxygen always remains higher, hence the oxygen concentration is also higher at

the TPB. It was observed that momentum conservation is important for high power range.

The pressure gradient ∇P can be approximately determined using Poiseuille's Law [104].

By calculating the friction factor f the wall shear stress yields:

$$f = \frac{2\tau}{\rho u^2} \tag{30}$$

f is constant for laminar flow and for turbulent flow it depends on Reynolds number and surface roughness [81].

In the case of the channel volume that is represented by porous medium (for the case of effective parameters) Darcy equation can describe the balance between the force from the pressure gradient ∇P and the frictional resistance ε from the solid material which is given by:

$$-\nabla P = \frac{\mu_g \varepsilon}{K} U_p \tag{31}$$

where U_p is the pore velocity vector, ε is the porosity (the volume fraction of void space), μ_g is the dynamic viscosity of the gas mixture and K is the permeability which depends on micro-structure of the porous electrodes.

For random packing systems of spherical particles, Caman-Kozeny correlation is generally used to evaluate the flow permeability as:

$$K = \frac{\varepsilon^3}{k_K (1-\varepsilon)^2 A_0^2} \tag{32}$$

where the Kozeny constant k_k is about 5 for porous media made of spherical particles.

A_0 is the specific area based on the solid volume:

$$A_0 = \frac{6}{d_{el}} \frac{n_{el} + (1-n_{el})\alpha^2}{n_{el} + (1-n_{el})\alpha^3} \tag{33}$$

α is bi-model size distribution.

The volume flow rate per unit area through the porous structure is obtained by multiplying U_p. The pore Reynolds number is defined by:

$$Re_p = \frac{\rho_g \left| U_p \right| d_p}{\mu_g} \tag{34}$$

where ρ_g is the gas mixture density. Eq. (34) is valid for $R_{ep} < 1$ [105] when pressure loss is dominated by pore friction and the inertia terms usually present in a momentum equation are insignificant. The Darcy equation describes the flow in the porous structure well away from the walls. It cannot model a no-slip condition at a wall nor the resulting boundary layers. It is found that, although the boundary layer thicknesses are typically only about 1–3% of the ceramic support thickness, Eq. (31) can be modified to allow their calculation. This is done by adding the so-called 'Brinkman' term to the Darcy equation which then becomes:

$$-\nabla P = \frac{\mu_g \varepsilon}{K} U_p - \nabla.(\mu_g \nabla) U_p \tag{35}$$

where the normal stresses in the final term as usual are ignored. Darcy equation was used by several researchers like Yakabe et al. [21], Bove et al. [32], Ho et al. [46] and others [21,32,38,39,46,64,69,79,101–103,106,107].

Pressure drop in both anode and cathode sides was neglected by some authors like Shi et al. [85] Aguiar et al. [108,109] and others [78,85,96,97,108,110–113]. However, the temperature variation along the cell can be accurately predicted by considering the pressure gradient among the fuel cell [114]. At the cathode side, neglecting the pressure gradient can lead to make an error in calculating of concentration overpotential by about 10% under typical working conditions [66].

3.2. Model equations for subsystem 2 (SS2)

This subsystem for TSOFC includes the solid of injection tube and for PSOFC is the solid of the cathode side interconnector. In this subsystem mass and energy balances can be accounted.

3.2.1. Heat transfer model

(i) An energy balance for TSOFC in the injection tube (SS2) leads to:

$$m_{it} \frac{\partial C_{p_{it}} T_{it}}{\partial t} = Q_{conv}^{it} + Q_{cond}^{it} + Q_{rad}^{it} \tag{36}$$

where m is the mass and C_p is the heat capacity.

Convection heat transfer in SS2 for TSOFC is between inside injection tube and air flow and also between outside the injection tube and the air flow inside the SS3 and can be written as follows:

$$Q_{conv}^{it} = h_{it_i}(T_{air}^{inj} - T_{it_i}) + h_{it_o}(T_{air}^{cat} - T_{it_o}) \tag{37}$$

Heat transfers inside the gases and through the electrodes, electrolyte and interconnectors walls with conduction heat transfer, however, the thermal conductivity of gases is mainly very low (0.025 W/m K) [66]. Conduction heat transfer described by Fourier's equation which is given by:

$$Q_{cond} = \nabla K \nabla T \tag{38}$$

K is the thermal conductivity of the solid structure.

Subscript it_o is the outside of the injection tube.

Thermal radiation within tubular SOFC in SS2 occurs between injection tube and inside the cell tube walls which is given by eq (38):

$$Q_{rad}^{it} = \frac{\sigma}{R_{rad}}(T_{ct_i}^4 - T_{it_o}^4) \tag{38'}$$

R_{rad} is the radiation heat transfer resistance which is given by [80]:

$$R_{rad} = \frac{1-\varepsilon_{ct}}{\varepsilon_{ct}} + \frac{1}{F_{ct-it}} + \frac{1-\varepsilon_{it}}{\varepsilon_{it}} \frac{A_{it_o}}{A_{ct_i}} \tag{39}$$

(ii) An energy balance for PSOFC in the cathode side interconnector (SS2) leads to:

$$m_{\text{int},c} \frac{\partial C_{p_{\text{int},c}} T_{\text{int},c}}{\partial t} = Q_{conv}^{\text{int},c} + Q_{cond}^{\text{int},c} + Q_{rad}^{\text{int},c} \tag{40}$$

Convection heat transfer for PSOFC is between the solid of the air side interconnector and air flow in SS2 which is given by Eq. (41):

$$Q_{conv}^{cat} = h_{\text{int},c_i}(T_{air} - T_{\text{int},i}^{cat}) \tag{41}$$

Thermal radiation within PSOFC in SS2 occurs between air side interconnector and cathode wall as follows:

$$Q_{rad}^{\text{int},c} = \frac{\sigma}{R_{rad}}(T_{ct,c_o}^4 - T_{\text{int},i}^{cat^4}) \tag{42}$$

$$R_{rad} = \frac{1-\varepsilon_{cat}}{\varepsilon_{cat}} + \frac{1}{F_{cat-\text{int}}} + \frac{1-\varepsilon_{\text{int}}}{\varepsilon_{\text{int}}} \frac{A_{\text{int}}}{A_{cat}} \tag{43}$$

Because of the high operating temperatures of SOFCs (typically 800–1200 K), there has been some estimation that thermal radiation may be an important factor of heat transfer within them. Radiation heat transfer has been involved by Hajimolana and Soroush [22], Damm et al. [89], Aguiar et al. [108], Iora et al. [91], Jia et al. [115], Achenbach [116] and other several models in [26–28,35,44,51,61,75,77,83,89,91,96,97,108,110,115–120]. Detailed discussions of radiation heat transfer within SOFCs are given by Hajimolana and Soroush [22], Qi et al. [43], Ho et al. [46], Sánchez et al. [58], Damm et al. [89], Brus et al. [121], Wang et al.

[98], Calise et al. [122], Haynes [123]. However, some researchers ignored radiation heat transfer due to considering a uniform temperature everywhere in the cell [55], or because of assuming a thin wall of channels [124]. In Iwai, H., et al. [125] model it was not clear why the radiation heat transfer was not tacked into account. Wang et al. [126] and Yakabe et al. [31] neglected the effect of radiation heat transfer in their model due to a very small amount compared to other types of heat transfer.

In fact, the magnitude of thermal radiation depends on two parameters, temperature and the thickness of electrodes and electrolyte. At a greater temperature and a thicker of the layers, the radiative transfer becomes more significant as compared to other heat transfer components.

Calise et al. [122] presented a model of a tubular SOFC in which the radiation heat transfer was modeled in details. It was observed that radiation heat transfer has a strong effect on temperature distribution among the fuel cell (about 70%). The model was developed by removing some simplification used in the study of Companari [127] and Stiller groups [28]. In Companari [127] the radiation heat transfer between air injection tube and the SOFC tube was neglected while F. Calise group [122] considered that the radiative heat transfer is predominately through the radial distribution among the fuel cell tube and air injection and is strikingly important.

Sánchez et al. [58] performed a steady-state model of a tubular SOFC including convection and radiation heat transfers. Two models for convection heat transfer were studied. In the first model film coefficient was a function of local temperature and composition. The local value for the heat transfer coefficient and the thermal entry length of the cell is clear with this model. In the second model, an average value of the heat transfer coefficient for the whole length of the fuel cell channel was assumed. Based on this study, it was observed that a simple model can be used to evaluate the fuel cell performance with satisfactory accuracy, although there is a need to calculate local temperatures. For radiation heat transfer, two models were performed again. The first model accounted the radial radiation exclusively and thus, radiative exchange between adjacent cells is neglected. The second model considered the radiation completely in all directions. This causes to increase significantly the complexity of model. It was found that a simple model based on a constant film convective heat transfer coefficient and a simple radiation model is enough for predicting the fuel cell performance without internal information requiring and using a complicate model is not necessary. A complete heat transfer model, however, is necessary for evaluating the internal fuel cell temperature accurately.

Conduction heat transfer was tacked into account by Stiller et al. [28], Negata et al. [44], Ho et al. [45,46], Ferguson et al. [50], Sánchez et al. [58] and other researchers [28,44–46,50,58,63,67,75,77,78,89,92,99,101,102,108,110,115,117,128,129] in order to model the distribution temperature of fuel cell more accurately. However; no conduction heat transfer was used by Hajimolana and Soroush [22], Costamagna et al. [26], Burt et al. [27], Qi et al. [43] and Achenbach [116]. In this studies conduction heat transfer was neglected due to assuming a thin thickness of electrodes, electrolyte and interconnectors walls or to make simple the heat transfer modeling for calculating. It was also found that at low temperature the conductivity through the YSZ electrolyte becomes limiting [76].

3.3. Model equations for subsystem 3 (SS3)

This subsystem for TSOFC includes the air inside the space between the cell and injection tubes and for PSOFC includes the fuel side interconnector.

3.3.1. Mass transfer model

(i) A mass balance on the air inside SS3 for TSOFC takes the form:

$$\frac{\partial \rho_{air}^{cat}}{\partial t} + \nabla(u_{air}^{cat}\rho_{air}^{cat}) = -\nabla N_{O_2} \tag{44}$$

A mass balance on oxygen leads to:

$$\frac{\partial \rho_{air}^{cat} Y_{O_2}}{\partial t} + \nabla(u_{air}^{cat}\rho_{air}^{cat} Y_{O_2}) = -\nabla N_{O_2} \tag{45}$$

The effect of O_2 diffusion on cell voltage and current is not significant because the concentration of O_2 in the air is 21% [25,34].

3.3.2. Heat transfer model

(i) An energy balance for TSOFC inside the SS3 leads to:

$$\frac{\partial \rho_{air}^{cat} H_{air}^{cat}}{\partial t} = \nabla \Delta \rho_{air}^{cat} u_{air}^{cat} H_{air}^{cat} + Q_{conv}^{cat} + Q_{diff}^{cat} \tag{46}$$

which accounts for energy flowing into and out of SS3 with air ($\nabla \Delta \rho_{air}^{cat} u_{air}^{cat} H_{air}^{cat}$), convectional heat transfer and diffusional heat transfer via oxygen into the cathode (Q_{diff}^{cat}),

Convective heat transfers from the cell and injection tubes are as follows:

$$Q_{conv}^{cat} = h_{it_o}(T_{it_o} - T_{air}^{cat}) + h_{ct_i}(T_{ct_i} - T_{air}^{cat}) \tag{47}$$

(ii) An energy balance for PSOFC inside the SS3 leads to:

$$m_{\text{int},a}\frac{\partial C_{p_{\text{int},a}} T_{\text{int},a}}{\partial t} = Q_{conv}^{\text{int},a} + Q_{cond}^{\text{int},a} + Q_{rad}^{\text{int},a} + Q_{cond}^{\text{int},a} \tag{48}$$

Convection heat transfer for PSOFC is between the solid of the fuel side interconnector and fuel flow in SS7 and leads to:

$$Q_{conv}^{\text{int},a} = h_{\text{int},a_i}(T_{\text{int},i}^{ano} - T_{fuel}^{ch,a}) \tag{49}$$

where superscript *ano* denotes the anode side.

Thermal radiation within PSOFC in SS3 occurs between fuel side interconnector and anode side walls and is as follows:

$$Q_{rad}^{\text{int},a} = \frac{\sigma}{R_{rad}}(T_{ct,a_o}^{4} - T_{\text{int},i}^{ano^4}) \tag{50}$$

where subscript ct,a_o denotes the outside the anode side of the cell tube.

3.3.3. Momentum model

Momentum conservation on the air inside SS3 for TSOFC takes the form:

$$\frac{\partial(\rho_{air} u_{air}^{cat})}{\partial t} + (\nabla \rho_{air} u_{air}^{cat} u_{air}^{cat}) = -\nabla N_{O_2} M_{O_2} u_{air}^{cat} - \nabla P_{air}^{cat} + \nabla \tau_{air}^{cat} + F_{air}^{cat}. \tag{51}$$

3.4. Model equations for subsystem 4 (SS4)

This subsystem for both TSOFC and PSOFC is the cell tube including electrodes and electrolyte. Electrochemical reaction, reforming and shift reactions occur in this subsystem.

3.4.1. Electrochemical reaction

High SOFC performance depends on optimal electrochemical reactions and mass transport processes. Since experimental studies on SOFC are expensive, time-consuming and labor-intensive, quantitative mechanistic models for the cell PEN structure are essential for SOFC technology development. Electrochemical reaction occurs inside the fuel cell which as a result produces voltage and current. At cathode side oxygen ions (with a negative charge) migrate through the crystal lattice. The oxygen is supplied, usually from air, at the cathode. Hydrogen and/or carbon monoxide

(CO) in the fuel stream reacts with oxide ions (O^{2-}) from the electrolyte to produce water or CO_2 and deposit electrons into the anode. The electrons pass outside the fuel cell, through the load, and back to the cathode, where oxygen from the air receives the electrons and is converted to oxide ions, which are then injected into the electrolyte. Generating efficiencies can range up to ~60%. In one configuration, the SOFC consists of an array of tubes. Another variation includes a more conventional stack of disks. The high operating temperature of the SOFC offers the possibility of internal reforming. As in the molten carbon fuel cells, CO does not act as a poison and can be used directly as a fuel.

$$\text{Anode Side Reactions} \begin{cases} H_2 + O^{2-} \rightarrow H_2O + 2e \\ CO + O^{2-} \rightarrow CO_2 + 2e \\ CH_4 + 4O^{2-} \rightarrow 2H_2O + CO_2 + 8e \end{cases}$$

$$\text{Cathode Side Reaction} \left\{ O_2(g) + 4e \rightarrow 2O^{2-} \right.$$

The 1000 °C operating temperature of SOFCs requires a significant start-up time. The cell performance is very sensitive to the operating temperature. A 10% decrease in temperature can lead to a 12% drop in cell performance, because of a higher internal resistance to the flow of oxygen ions [46]. The high temperature also demands that the system include significant thermal shielding to protect personnel and to retain heat. Such requirements are acceptable in utility applications but not in small portable, transportable, or most transportation applications.

It is significant that a SOFC can use CO, as well as hydrogen as its direct fuel. When both species of H_2 and CO are present in the system, CO mostly participates in the water–gas shift reaction of equation [94] rather than in the electrochemical process [130]. However, current produces by the sum of hydrogen and carbon monoxide oxidation at the anode side by the electrochemica reaction. The rate of H_2 oxidation is 2–3 times more than that of CO oxidation depending on the operationg temperature [131]. Ho et al. [132] assumed that the rate of CO oxidation is 3 times less that of H_2 oxidation due to high operating temperature of the fuel cell. On the other hand, Hofmann et al. [130] assumed that only H_2 participate at electrochemical reaction due to its fast kinetic reaction.

It is noteworthy that when the shift reaction is at equilibrium condition, CO and H_2 oxidation produces the same Nernst potential in the fuel cell [131]. Many authors like Cayan et al. [40], Yakabe et al. [42], Qi et al. [43] and other researchers in [40,42,43,61,68,69,112,116,133–135] considered CO oxidation in their model to make their model more realistic. However, some researchers like Costamagna et al. [26], Stiller et al. [28], Ho et al. [46] and also [26,28,46,102,103,106,110,113,117,120,136–138] ignored occurrence of CO oxidation at the anode side due to dominating of H_2 over CO in the charge transfer chemistry It is estimated that about 98% of current is produced by H_2 oxidation in common situations and therefore CO seems to play a minor role and can safely be neglected [139].

Aloui and Halouani [69] compared the fuel cell performance with and without carbon monoxide oxidation at the anode side. It was observed by L. Petruzzi et al. [140] that CO oxidation at the electrochemical reaction influences the cell efficiency, fuel utilization, thermodynamic efficiency and electric power. Actually, oxidation temperature heavily depends on CO and as a result, CO oxidation can affect the cell performance.

Methane can also possibly be electrochemically oxidized in the case of absence or near-absence of steam feed [93,104]. However, with high content of steam the fast reforming reaction will dominate over any oxidation of methane and can safely be neglected.

Incidentally, a pure voltage source is usually referred to as an electromotive force (emf). The electromotive force, reversible open-circuit cell voltage (denoted by U_{OCV}) is given by the Nernst equation:

$$U_{OCV} = U^0(T) + \frac{RT}{2F} \ln \left[\frac{x_{H_2,a} x_{O_2}^{0.5} (P_c/P^{ref})^{0.5}}{x_{H_2O,a}} \right] \quad (52)$$

Equation [52] is hold for hydrogen, where U_{OCV} is the standard potential cell, R is the universal gas constant, F is Farady constant, P is the pressure, $U^0(T)$ is the standard cell potential, and x is the mole fraction. If the shift reaction is assumed to be at equilibrium the U_{OCV} of Co is equal to that of CO.

In practice, cell emf depends on temperature and concentration of reactants and products. If the concentration of reactants increases relative to the products, the cell reaction becomes more spontaneous and the emf increases. As the cell operates, the reactants are used up as more product is formed causing the emf to decrease.

For a fuel including H_2 and CO the ideal potential for reaction using the Nernst equation is as follows:

$$U_{OCV} = U^0(T) + \frac{RT}{n_e F} \left\{ n_{H_2} \ln\left(\frac{P_{H_2}}{P_a}\right) + n_{CO} \ln\left(\frac{P_{CO}}{P_a}\right) - n_{H_2} \ln\left(\frac{P_{H_2O}}{P_a}\right) - n_{CO} \ln\left(\frac{P_{CO_2}}{P_a}\right) + n \ln\left(\frac{P_{O_2}}{P_c}\right) \right\} \quad (53)$$

n_e is the total number of electrons transferred and given by [49]:

$$n_e = n_{H_2} \times 2 + n_{CO} \times 2 \quad (54)$$

However, the actual cell voltage (U) is less than its theoretical open circuit voltage because it strongly affected by several irreversible losses including activation losses due to irreversibility of electrochemical reactions at the three-phase boundary, concentration losses due to mass transport resistance in the electrode, especially for thick anodes as in an anode-supported SOFC [50] and ohmic losses due to ionic and electronic charge transfer resistances. Actual voltage is given by:

$$U = U_{OCV} - \eta_{ohm} - \eta_{act} - \eta_{conc} \quad (55)$$

The rates of consumption of hydrogen and oxygen by the electrochemical reactions to generate an electric current of I are given by:

$$R_{H_2} = \left(\frac{1}{2F}\right) j \qquad R_{O_2} = \left(\frac{1}{4F}\right) j \quad (56)$$

The consumption of the reactants is accompanied by the production of water at the following rate:

$$R_{H_2} = \left(\frac{1}{2F}\right) j. \quad (57)$$

3.4.2. *Electrochemical losses*

3.4.2.1. Activation Losses. The activation polarizations are the results of the kinetics involved with the electrochemical reactions. It becomes an important loss when the current is low because at low current density (j) the reactants must overcome an energy barrier named activation energy (E_{sct}) to drive the electrochemical reactions at the electrodes–electrolyte interface and this barrier leads to the polarization. The activation barrier is the result of many complex electrochemical reaction steps where, typically, the rate-limiting step is responsible for the polarization. One can account

for the anode and cathode activation polarizations using the well known Butler-Volmer equation [30]:

$$j = j_0\left\{\exp\left(\frac{\alpha\eta_{act,i}n_iF}{RT}\right) - \exp\left(\frac{-(1-\alpha)\eta_{act,i}n_iF}{RT}\right)\right\} \quad (58)$$

The equation explains the net anodic and cathodic current density due to an electrochemical reaction. Where subscript i represents the species H_2, CO and O_2, j is the current density, n is the number of electrons transferred in the electrochemical reactions, η_{act} is the activation polarization, α is the transfer coefficient and its value is usually 0.5, and j_0 is the exchange current. When $\beta = 0.5$, Eq. (58) can be expressed as follows:

$$j = 2j_0 \sinh\left(\frac{n_iF\eta_{act,i}}{2RT}\right) \quad (59)$$

The total current density is given by:

$$\begin{aligned} j_{tot} &= j_{O_2} \\ j_{tot} &= j_{H_2} + j_{CO} \end{aligned} \quad (60)$$

At the equilibrium potential the electrode/electrolyte interface still has electron transfer processes going on in both directions. The ongoing current in both directions at the dynamic equilibrium electric potential differences is called exchange current density. The exchange current density is a factor to measure the electrocatalytic activity of TPB for a given electrochemical reaction. It is also a significant factor for calculating the activation polarization. Exchange current density depends on many parameters such as concentration of reactants and products at the electrodes, temperature, pressure, the microstructure and electrocatalytic activity of the electrode, and even conductivity of electrolyte [104]. Exchange current density with respect to reactant concentrations dependency can be calculated as follows [30]:

$$j_0 = j_0^0 \prod_{K=1}^{K} X_K^{\gamma_k} \quad (61)$$

where j_0^0 is a constant, and γ_k and X_K are the reaction order and mole fraction (at the electrode–electrolyte interface) for the Kth species, respectively [30,62]. A high exchange current density causes the reaction to occur rapidly, so a good fuel cell performance can be expected.

Solving the Butler-Volmer equation with a transfer coefficient of 0.5 in the high-current-density regime (where the cell typically operates) leads to:

$$\begin{aligned} \eta_{act,a} &= \left(\frac{RT}{n_iF}\right)\sinh^{-1}\left(\frac{j}{2j_{0,a}}\right) \\ \eta_{act,c} &= \left(\frac{RT}{n_iF}\right)\sinh^{-1}\left(\frac{j}{2j_{0,c}}\right) \end{aligned} \quad (62)$$

where $j_{0,a}$ and $j_{0,c}$ are the anode and cathode exchange currents.

$E_{act,ano}$ and $E_{act,cat}$ are energy activation of anode and cathode, P^{TPB} is the pressure of components inside the triple phase boundary, and A is the surface area of the cell.

High activation polarization and low activation polarization are two possible cases of Eq. (58). Under high activation polarization, the first term of Eq. (58) will be much greater than the second term, so the simplified equation is given as follow:

$$\eta_{act,i} = \left(\frac{RT}{\beta n_iF}\right)\ln\left(\frac{j}{j_0}\right) \quad (63)$$

which is called the Tafel equation.

At low activation polarization, the term $(\alpha\eta_{act,i}F/RT)$ in Eq. (58) will be much less than and the exponential terms can be expanded as a Taylor series. Therefore, by ignoring the terms with order higher than unity the following equation yields:

$$\eta_{act,i} = \left(\frac{RT}{n_iFj_0}\right)j \quad (64)$$

which is a relation that shows linear current potential. The issue of applying the range of activation polarization for using the Tafel equation or linear current relation is discussed by S.H. Chan et al. [30].

Activation polarization in high temperature for the case of SOFCs is usually small [141]. It also depends on CO and H_2 concentration and decreases when the amount of these components in fuel increases due to the amelioration of the anode exchange current density.

3.4.2.2. Concentration losses. Concentration losses are losses associated with concentration variation of the critical species due to mass transport processes. There are usually two sources of loss that are due to mass transport loss: (i) diffusion between the bulk flows and cell surfaces, and (ii) transport of reactants and products through electrodes. Therefore, the concentration polarization is highly dependent on the gases used, as well as the distance through which the gases must diffuse. Pore volume percentage, as well as diffusion length, can be varied to optimize these properties. For similar geometries, cathode concentrations are much larger than anode concentrations, because of the lower diffusivities of O_2/N_2 in the cathode than H_2/H_2O in the anode. The anodic and cathodic concentration losses can be calculated, respectively, as the following:

$$\begin{aligned} \eta_{conc,a} &= \frac{RT}{n_eF}\sum_{i=1}^{i}(\nu'_f n_{f,i} - \nu''_{f,i})\ln\left(\frac{[X_i]^*}{[X_i]^s}\right) \\ \eta_{conc,c} &= \frac{RT}{n_eF}\sum_{i=1}^{i}(\nu'_a n_{a,i} - \nu''_{a,i})\ln\left(\frac{[X_i]^*}{[X_i]^s}\right) \end{aligned} \quad (65)$$

where X_i is the component symbol for the ith species which may be involve in the fuel or oxidizer. ν'_f and ν'_a are the stoichiometric coefficients for the fuel and oxidizer mixtures, respectively, and $\nu''_{f,i}$ and $\nu''_{a,i}$ are the stoichiometric coefficients of the ith product species in the fuel and air channels, respectively. $[X_i]^*$ and $[X_i]^s$ denote the molar species concentration in the channels and triple phase boundary, respectively.

This type of polarization loss is considerable for high fuel utilization [142] also normally reduced at high current density. A dramatic change happens for an anode-supported tubular SOFC which requires high fuel utilization due to a small error in the concentration overpotential calculation.

3.4.2.3. Ohmic losses. Ohmic losses happen due to existence of resistance for ions transferring through the electrolyte and electrons through the electrodes and current collectors and by contact resistance between the cell components. Ohmic losses can be calculated as follows:

$$\eta_{ohm} = R_{tot}i \quad (66)$$

where R_{tot} is the total area specific resistance and can be calculated as follows [142]:

$$R_{tot} = \left[\left(\frac{\delta_a}{\sigma_a}\right) + \left(\frac{\delta_e}{\sigma_e}\right) + \left(\frac{\delta_c}{\sigma_c}\right)\right] \quad (67)$$

where δ is the thickness, and a, c and e denote the anode, cathode and electrolyte, respectively, and σ is the conductivity of electrodes

and electrolyte which is defined as a function of temperature as follows [143]:

$$\sigma_e = 3.34 \times 10^4 \exp\left(-\frac{10300}{T}\right)$$

$$\sigma_a = \left(\frac{95 \times 10^6}{T}\right) \exp\left(-\frac{1150}{T}\right)$$

$$\sigma_c = \left(\frac{42 \times 10^6}{T}\right) \exp\left(-\frac{1200}{T}\right) \quad (68)$$

The above equations are valid for the YSZ electrolyte material [144].

Hajimolana and Soroush [22] and Qi et al. [34,43] assumed a constant value for specific resistance while Costamagna et al. [26], Stiller et al. [28] and other many research studies calculated the anode/electrolyte/cathode resistance [25,26,28,69,110, 133,145].

In order to evaluate ohmic losses, some authors [28,59] used the Nisancioglu's expression, Eqs. (69)–(74) [146], with a correction for the ionic/electric resistivity dependence on temperature, Eq. (74) giving by:

$$\Delta V_{ohm,j} = \frac{j_j A_{slice} R_{eq,j}}{L_{slice}}, \quad (69)$$

where

$$R_{eq} = R_{eq,1} + R_{eq,2}, \quad (70)$$

$$R_{eq,1} = \frac{((\rho_a/\delta_a)^2 + (\rho_c/\delta_c)^2 \cosh(Z_e) + \rho_a\rho_c/\delta_a\delta_c(2 + Z_e \sinh(Z_e)))}{2(1/\rho_e\delta_e)^{1/2}(\rho_a/\delta_a + \rho_c/\delta_c)^{3/2}\sinh(Z_e)}, \quad (71)$$

$$R_{eq,2} = \frac{\sqrt{\rho_{icm}\delta_{icm}(\rho_c/\delta_c)}}{2\tanh(L_{icm}/2\sqrt{(\rho_c/\delta_c)/\rho_{icm}\delta_{icm}})}, \quad (72)$$

$$Z_e = \frac{L_e}{2}\sqrt{\frac{1}{\rho_e\delta_e}\left(\rho_a/\delta_a + \rho_c/\delta_c\right)}, \quad (73)$$

$$\rho_i = \frac{T}{C_{1,i}} \exp\left(\frac{C_{2,i}}{T}\right). \quad (74)$$

In these equations A is the active area, j_j the current density, $R_{eq,j}$ is equivalent ohmic resistance, L is the slice length, ρ ohmic resistance, δ thickness and C resistivity.

Several SOFC models have been developed to study polarization losses within the PEN structure.

Hirano et al. [146] presented a model in order to investigate the effect of concentration/ohmic polarization on electrochemical model by assuming that the activation polarization is negligible.

Burt et al. [27], Ji et al. [29], Chan et al. [30], Izzo Jr et al. [38] and other many papers like [25,27,29,30,38,41,66, 74,77,78,83,97,108,110,115,117,120,134,147–151] performed the three activatin/concentration/ohmic polarizations in their model.

Tanaka et al. [152], Aguiar et al. [108] and Achenbach [116] considered only the activation polarization in their model.

In the Aguiar et al. [108] survey, it was assumed that except for the shift reaction the principle electrochemical reactions are considered kinetically controlled, and therefore only the activation overpotentials were taken into account. It was assumed that the other overpotentials are small and can be ignored.

Chaisantikulwat et al. [39], Ho et al. [45], Bhattacharyya et al. [54], Janardhanan et al. [67], Danilov et al. [99] and Wang et al. [98] accounted both activation and ohmic losses in their model and neglected the concentration polarization.

Activatioin and ohmic polarization were accounted by Ota et al. [34]. In the study it was also assumed that concentarion gradient in the gas phase exists only in the porous electrodes.

Padulleĭs et al. [153] neglected the activation/concentration polarization and only considered to ohmic loss in their model while Yakabe et al. [42] considered only concentration polarization in their model.

In recent years, several SOFC models have been developed by Chan et al. [30], Sánchez et al. [59], Nam et al. [64], Klein et al. [90] and other studies in [30,55,59,62–64,85,86,90,136,148,150,154] to investigate reactions and transport phenomena within the PEN structure. These models differ widely in terms of their complexity and comprehensiveness.

Chan et al. [30] performed a complete polarization model. In this paper the effect of electrodes and electrolyte thicknesses was studied. It was observed that the sensitivity of cell voltage due to change of electrolyte thickness is the highest, then sensitivity of cell voltage due to the change of cathode thickness and finally the sensitivity of cell voltage due to the change of anode thickness. Reducing all three component thicknesses causes, in general, reduced sensitivity strength with an improved operating current density range. However; considering both current density and PEN thicknesses is significant and needs an optimization between both factors in order to obtain a high performance while in this paper both factors was issued. A cathode-supported cell is no way better than an anode-supported cell for high performance fuel cell design even under elevated pressure conditions at the cathode compartment to compensate for the serious cathode concentration overpotential loss. It was illustrated that the cell potential losses is mostly due to anode side of the cell in an anode-supported SOFC.

Nam et al. [64] illustrated a comprehensive micro-scale model for explaining the transport phenomena and reaction in SOFCs. They showed that the potential loss in cathode was considerable at all current densities while the potential loss in anode was negligible at low current densities and important at higher current densities. Based on their research, it was observed that the size of particle has the most significant impact on the PEN performance optimization. By increasing the length of TPB in the electrodes and smaller particle size, the activation overpotential will be reduced, while at the same time by decreasing Knudsen diffusivity and flow permeability the mass transport resistance increases. On the other hand, the volume fraction of electronic phase of around 0.45 was found optimal for both anode and cathode for the same ionic and electronic particle size. Higher porosity in anode and lower porosity in cathode gives a better PEN performance. The porosity, particle size, and thickness of electrodes were found to have conflicting effects on the PEN performance. For example, by decreasing the particle size of electrodes the efficiency of electrochemical reaction increases while the efficiency of mass transport decreases. An optimal set of micro-structural parameters, which resulted in best PEN performance, will not automatically result in best SOFC performance. Micro-structural optimization of SOFC performance requires consideration on the interconnect rib geometry and the flow field effects, in addition to the detailed micro-scale calculation in PEN. In the paper also the effect of electrodes thickness was investigated in details. It was also depicted that with a larger of electrode thickness the performance increases, however; at higher current density the effect of electrode thickness will be negligible.

Jiang et al. [148] modeled a one-dimensional dynamic model of a TSOFC stack. It was found that higher operating temperature decreases both the Nernst potential and the irreversible losses, resulting in an initial increase then a decrease in cell efficiency. In this paper the resistivity and ohmic losses in different layers of

tubular SOFC were calculated as follows:

$$\begin{aligned} &\rho = 0.00298\,e^{-1392/T} \text{ fuel electrode} \\ &\rho = 0.00294\,e^{10350/T} \text{ electrolyte} \\ &\rho = 0.008114\,e^{600/T} \text{ air electrode} \\ &\rho = 0.12568\,e^{4690/T} \text{ interconnect} \end{aligned} \quad (75)$$

$$R = \rho.\frac{L}{A} \quad (76)$$

Jiang et al. also studied the effect of fuel cell size like fuel cell diameter and length. It was represented that by an increase of cell diameter the power increase due to a larger activation area at the same time and also the ohmic loss increase due to longer current path length.

Ni et al. [66] developed an electrochemical model for studying the ammonia (NH_3)-fed solid oxide fuel cells with proton-conducting electrolyte (SOFC-H) and oxygen ion-conducting electrolyte (SOFC-O). It was observed that the actual performance of the NH_3-fed SOFC-H is significantly lower than SOFC-O, mainly due to higher ohmic overpotential of the SOFC-H electrolyte. It was also presented that compared with the NH_3-fed SOFC-H, the SOFC-O has higher anode concentration overpotential and lower cathode concentration overpotential. The effects of temperature and electrode porosity on concentration overpotentials were also studied in order to identify possible methods for improvement of SOFC performance. This study observed that the use of different electrolytes not only causes different ion conduction characteristics at the electrolyte, but also significantly influences the concentration overpotentials at the electrodes.

Ni et al. [41] investigated the effect of micro-structures of electrodes on SOFC performance. A mathematical model for a planar SOFC was developed for studying the effects of varies parameters on the fuel cell performance. Nam et al. [64] work, they revealed that both porosity grading and pore size grading can effectively improve the SOFC performance. Based on this survey, at low current density SOFC potential decreases with increasing porosity, while at high current density, optimal porosity was found and the optimal porosity increases with increasing current density. Moreover; the effect of pore size and porosity of electrodes on the overpotentials was studied while this effect was not considered by Nam et al. [64] work. Based on their results, variation of porosity has an inverse influence on activation and concentration overpotentials. Similar to porosity, the electrode pore size has opposite effects on activation and concentration overpotentials. The mechanisms of coupled transport and chemical reactions in the porous electrodes and evaluated possible ways to improve SOFC performance were also studied. The model developed in the paper can be effectively applied to the SOFC design optimization to maximize the energy efficiency of CH_4 fed SOFC for clean power generation. In addition; the impact of CH_4 fed SOFC on overpotentials was studied. Regarding this study, for SOFC fed by CH_4, all the overpotentials decrease with increasing temperature while in H_2 fed SOFC the concentration overpotential slightly increases with increasing temperature. The effect of methane reforming and water-gas shift reactions is significant at high temperature, resulting in high rate of H_2 production and high molar ratio of H_2 and H_2O.

Arpino et al. [74] investigated the effect of current density and fuel utilization on the overpotential losses. Based on their research, both concentration and activation polarizations at the anodic compartment increase significantly for a high value of current density. It was also observed that there are no important gradients in the anodic concentration polarization at lower current density as the inlet hydrogen velocity varies.

Table 6 illustrates some papers that concerned on PEN in their model.

3.4.3. Mass transfer model

At the electrodes, hydrogen and oxygen in the case of pure hydrogen as a fuel, diffuse from anode and cathode sides, respectively, into the triple phase boundary for occurring electrochemical reaction, and then after the products diffuse into the anode side. The diffusion of components from fuel channel into the TPB depends on the type of the fuel fed to the SOFCs. Mass transport models inside the electrodes are giving an accurate prediction for gas concentration at the anode-electrolyte-cathode interface. Therefore; an accurate modeling of this phenomenon is imperative for development of better fuel cell designs.

A mass balance on oxygen inside the cathode-side diffusion layer yields:

$$\frac{\Delta_{cat}}{R}\frac{\partial}{\partial t}\left[\frac{P_{O_2}^{TPB}}{T_{ct_{TPB}}}\right] = \nabla N_{O_2} - \frac{R_{O_2}}{A_c} \quad (77)$$

Δ_{cat} is the thickness of the cathode layer, R is the universal gas constant, P_i^{TPB} is the pressure of component at TPB, A_c is the surface area of cathode side and $T_{ct_{TPB}}$ is the cell tube temperature at *TPB*.

By assuming that synthesis gas is as a fuel fed to SOFC, mass balances on hydrogen and water vapor inside the anode-side diffusion layer yield are given as follows:

$$\frac{\Delta_{ano}}{R}\frac{\partial}{\partial t}\left[\frac{P_{H_2}^{TPB}}{T_{ct_{TPB}}}\right] = \nabla N_{H_2} - \frac{R_{H_2}}{A_a} \quad (78)$$

$$\frac{\Delta_{ano}}{R}\frac{\partial}{\partial t}\left[\frac{P_{H_2O}^{TPB}}{T_{ct_{TPB}}}\right] = -\nabla N_{H_2O} - \frac{R_{H_2O}}{A_a} \quad (79)$$

Δ_{ano} is the thickness of the anode layer, A_a is the surface area of anode side.

3.4.4. Heat transfer model

Cell temperatures influence the electrochemical model and these temperatures affect the local driving voltage, polarizations, and heat generation within the cell.

(i) An energy balance inside the SS4 for TSOFC leads to:

$$m_{ct}\frac{\partial C_{p_{ct}} T_{ct}}{\partial t} = Q_{conv}^{ct} + Q_{cond}^{ct} + Q_{rad}^{ct} + Q_{diff}^{ct} + Q_{elc} \quad (80)$$

Convection heat transfer inside the SS4 for TSOFC is between inside the wall of the cell tube and air flow inside the SS2 and outside the wall of cell tube and fuel flow which is given by:

$$Q_{conv}^{ct} = h_{ct_i}(T_{air}^{inj} - T_{ct_i}) + h_{ct_o}(T_{fuel}^{ano} - T_{ct_o}) \quad (81)$$

Thermal radiation within tubular SOFC in SS4 occurs between injection tube and inside the cell tube walls which is given by:

$$Q_{rad}^{ct} = \frac{\sigma}{R_{rad}}(T_{it_o}^4 - T_{ct_i}^4) \quad (82)$$

For both TSOFC and PSOFC in SS4, O_2 and H_2 diffuse into the cathode and anode, respectively, in order to participate in electrochemical reaction, and H_2O is the electrochemical production that diffuses from cell tube into the fuel channel. Thus the diffusional heat transfer leads to:

$$Q_{diff}^{cat} = \sum \nabla N_i H_i \quad (83)$$

In the case of synthesis gas as a fuel, O_2, H_2, and CO diffuse into the cell tube, and H_2O diffuses into the fuel channel.

In the case of electrochemical heating (Q_{elec}), heat generates by the reversible and irreversible processes inside the electrodes and electrolyte within the triple phase boundary. Reversible heat generation is due to entropy transfer by the electrochemical reactions at the cathode and anode side which

Table 6
Selected studies concerning on PEN model of SOFCs.

Author	Cell type	Objective	Method	Short coming	Assumption
F. Zhao et al. [158]	PSOFC	To anticipate the concentration polarization in detail.	Porous media gas phase transport processes based on Fick's model was considered for predicting the concentration over potentials.	The models are limited to particular cells and cannot describe the effects of operating and design parameters in detail.	1D
N. Autissier et al. [35]	PSOFC	To predict current density, flow, temperature and concentration fields in order to compare and optimize repeat element geometry for a whole stack.	A commercial CFD tool was used, solving mass, momentum and energy equations; whereas chemical kinetic equations were computed from external sub-routines, Radiative heat transfer was accounted between inner surfaces.	The model parameters are not determined from experiments or from literature, they were only estimated.	1D steady state, laminar for both fuel and air flow
Shi et al. [86]	PSOFC	To investigate the intricate interdependency among the ionic conduction, electronic conduction, multi-component species transport, electrochemical reaction processes and electrode microstructure for intermediate temperatures operation. between 750 and 850 °C	The model was calibrated using experimental polarization curves and then validated by comparing each cell component polarizations (anodic, cathodic and electrolyte)	-Convection flux was neglected in the porous electrode compared to diffusion. - Pressure gradients in the porous electrode were neglected. - All physical properties were evaluated at a fixed cell temperature.	2D steady state, isothermal
Xie and Xue. [87]	anode-supported solid oxide fuel cell	To de-convolute the complicated transient interactions among operating conditions, internal multi-physics processes, and SOFC current responses.	The model was tacked into account the complex transport phenomena within PEN assembly, including charge (ion/electron) migration and species transport.	The pressure gradient within porous electrodes was neglected	Isothermal 2-D transient

is exothermic and slightly endothermic, respectively [155] which is given by:

$$Q_{rev,a} = T_{ct_{TPB}}(2S_{H_2O} - 2S_{H_2} + 4S_{e^-})\frac{j}{4F} \quad (84)$$

$$Q_{rev,c} = T_{ct_{TPB}}(2S_{O^{2-}} - 2S_{O_2} - 4S_{e^-})\frac{j}{4F} \quad (85)$$

where S_e is the molar entropies of the products and reactants at the operating temperature and pressure.

Irreversible heat generation at the anode and electrolyte region is caused by anodic and cathodic overpotentials which are given by:

$$Q_{irr,a} = j\eta_a \quad (86)$$

$$Q_{irr,c} = j\eta_c \quad (87)$$

Heat also generates by the ohmic heating in the electrodes and electrolyte due to existing of resistances to flow of ions and electrons which is given by:

$$Q_{ohm} = \rho_e j^2 \quad (88)$$

where ρ_e is the ionic resistivity of the electrolyte. It is reported that ohmic heating is about 2.37–4.1% of the total heat produced in an electrolyte-supported planar SOFC [156]. However, Andreassi et al. [129] assumed that the ohmic heating in the porous electrodes is negligible because of high electrical conductivity as compared to the ionic conductivity.

All the heat sources generated by electrochemical reaction are determined by Bove et al. [32], Klein et al. [90], Ni et al. [103], Young et al. [104] and studies in [25,32,39,90,103,104,106,126,129,131,157,158].

(ii) An energy balance inside the SS4 for PSOFC leads to:

$$m_{ct}\frac{\partial C_{p_{ct}}T_{ct}}{\partial t} = Q^{ct}_{conv} + Q^{ct}_{cond} + Q^{ct}_{rad} + Q^{ct}_{diff} + Q_{elc} \quad (89)$$

Convection heat transfer inside the SS4 for PSOFC is between the wall of the cathode side and air flow inside the SS1 and the wall of the anode side and fuel flow which is given by:

$$Q^{ct}_{conv} = h_{ct,c_o}(T_{air} - T_{ct,c_o}) + h_{ct,a_o}(T^{ch,a}_{fuel} - T_{ct,a_o}) \quad (90)$$

Thermal radiation within planar SOFC inside the SS4 occurs between cathode side of cell tube and air side interconnector walls, and also between anode side of the cell tube and fuel side interconnector walls which is given by:

$$Q^{ct}_{rad} = \frac{\sigma}{R_{rad}}(T^{ano4}_{\text{int},i} - T^4_{ct,a_o}) + \frac{\sigma}{R_{rad}}(T^{cat4}_{\text{int},i} - T^4_{ct,c_o}) \quad (91)$$

In some works, radiation heat transfer was neglected in the planar SOFC because in these works it was shown that this type of heat transfer has only a negligible effect on the temperature field within the electrode and electrolyte [155,159,160].

Large variations in the cell performance occurs when only conductive and convection heat transfer among the fuel cell stack is considered, while by adding the radiation heat to the model, the uniformity of temperature promotes within the

Table 7
Selected studies concerning on novel solid oxide fuel models.

Author	Objective	Method	Results and advantages of the model
Entchev, E et al. [192]	To predict SOFC performance while supplying both heat and power to a residence.	Applied adaptive neuro-fuzzy inference system (ANFIS) techniques and artificial neural network (ANN)	-The prediction of both ANN and ANFIS models was well in agreement with variety of experimental data. -Compared to the conventional models the ANN and ANFIS models are able to predict and optimize system performance faster and deliver better results in many instances. -the ANFIS model predicts the fuel cell current better than ANN model. -The ANN model predict the fuel cell voltage better than the ANFIS model.
Wu et al. [197]	To describe the nonlinear temperature and voltage dynamic properties of the SOFC system	It was applied Takagi–Sugeno (T–S) fuzzy model.	- The relationship between inputs and outputs of the SOFC system can be predicted while the complicated inner structure was ignored.
Arriagada et al. [198]	To evaluating the SOFC performance	Used an Artificial neural network method	-The SOFC model based on ANN was well in agreement with the physical model. -ANN model was much easier and faster to use compared to mathematical model.
Yang et al. [199]	To control fuel cell temperature	A modified Takagi–Sugeno (T–S) fuzzy modeling study was presented.	-The modified T-S fuzzy model simplified the complicated mathematical model and quickly made an accuracy relationship between inputs and outputs of the system. -Based on the results the modified T-S fuzzy yielded a high accuracy over a relatively wide operating temperature range
Wu et al. [200]	To facilitate a valid control strategy design	A radial basis function (RBF) neural network based on a genetic algorithm (GA) was applied.	-The results were congruence in agreement with simulation results. - It was possible to design an online controller of a SOFC stack based on this GA-RBF neural network identification model.
Hua et al. [201]	-To facilitate a valid control strategy design. - Trying to avoid the complexities of model based on conversion laws	Performed a black-box model of the SOFC based on least squares support vector machine (LS-SVM)	-The LS-SVM was superior to the conventional RBFNN in predicting stack voltage with different fuel utilizations.

stack, thus leads to more uniform the cell voltage. The variation of cell-to-cell voltage is less than 0.2% in the model that is involved radiation heat transfer and 0.3% in the model without radiation [27]. In the case of indirect internal reforming, that radiative heat transfer accounts for up to 79% of the total heat transfer between the solid structure and the reformer [108].

3.4.5. *Reforming and shift reactions*

Reforming reaction of hydrocarbons such as methane or natural gas is a process for producing the hydrogen required by fuel cell. This reaction is predominately performed between 600 and 900 °C and is thus compatible with SOFCs. The heat produced in a fuel cell can provide the heat for the endothermic reforming reaction. Therefore, with elaborating an appropriate catalyst using in anode manufacturing, internal reforming reaction in fuel cell can eliminate the requirement for indirect internal fuel reformer and is expected to simplify the overall system design and finally the economical cost of these power systems will decrease substantially. By manipulating the internal reforming reaction the fuel cell temperature can decrease to a suitable temperature. There are two alternate internal reforming within a SOFC: indirect (IIR-SOFC) and direct (DIR-SOFC) internal reforming. In the former process the reformer part is separate but adjacent to the anode cell. In the second process, methane is fed directly into the cell and the reaction occurs on the anode. However, this process has two major problems. One problem is that internal reforming is highly endothermic and thus cell temperature drops initially and then increases again, hence generate large temperature gradients across the cell, as well as a drop in cell performance. Deactivation of the anode by carbon formation at intermediate temperature and high pressure is the second problem of the DIR-SOFC which reduces the system efficiency. The problem, however, can be solved by adding H_2O or CO_2 into the syngas fuel. The complete steam reforming reaction takes place according to Eq. (92)

$$CH_4 + 2H_2O \rightarrow 4H_2 + CO_2 \quad (92)$$

Reforming reaction mainly occurs in the diffusional layer of anode or in the electrochemically active layer. But the rate of the reaction in the latter layer is assumed to be much lower than the former layer because of competition with the electrochemical reaction which includes much more hydrogen.

Eq. (92) is the combination of two independent reactions: methane steam reforming, Eq. (93), and water gas shifting, Eq. (96), which are highly endothermic and slightly exothermic, respectively:

$$CH_4 + H_2O \rightarrow 3H_2 + CO \quad (93)$$

$$CO + H_2O \rightarrow H_2 + CO_2 \quad (94)$$

The shift reaction assumed to tacke place always at the anode layer.

Although Eqs. (93) and (94) occur, the following carbon forming reactions may also appear in the anode and the pre reformer:

$$CH_4 \rightarrow C + 2H_2 \tag{95}$$

$$2CO \rightarrow C + CO_2 \tag{96}$$

These two reactions are endothermic and exothermic, respectively. If any of these two reactions take place at the anode, deposition of carbon particles over the anode surface will deactivate the catalyst and thus reduce the cell performance. At high temperature around 1000 K, methane is more likely to react with steam to form hydrogen according to Eq. (92) than to dissociate into atomic carbon and water [150]. This reaction increases when the steam concentration is high. For carbon monoxide, decomposition occurs when the steam concentration is not high enough. Shift reaction is clearly dominant by the excess steam in the fuel stream.

Many researchers like Hajimolana and Soroush [22], Ni et al. [41], Qi et al. [43], Nikooyeh et al. [48], Suwanwarangkul et al. [52] and also other researchers in [22,41,43,48,52,65,67,69,91,97,98,110,150,161,162] considered DIR-SOFC in their model.

Yingwei et al. [97] observed that direct internal reforming process has significant effect on the distributions of the anode gas composition, cell temperature, solid temperature gradient, and current density along the cell length direction.

Dokamaingam et al. [77,78], Brus et al. [121], Aguiar et al. [108,109] modeled IIR-SOFC in their system.

3.4.5.1. Equilibrium model. Few authors considered that the reforming and shift reaction are equilibrium inside the cell [163,164]. The constant equilibrium for reforming and shift reactions yield with the [99,100] equations which depend on temperature exponentially as depicted in Eq. (100), where subscript i stands for both reforming and shift reactions. The constant values are reported in [163,164] which are given by:

$$K_{eq,ref} = \frac{P_{H_2}^3 P_{CO}}{P_{CH_4} P_{H_2O}} \qquad K_{eq,shift} = \frac{P_{H_2} P_{CO_2}}{P_{H_2O} P_{CO}} \tag{97}$$

$$\log K_{eq,i} = a_i T_{ct}^4 + b_i T_{ct}^3 + c_i T_{ct}^2 + d_i T_{ct} + e_i \tag{98}$$

which both the reforming and shift reactions occur at the surface of the anode side.

Suwanwarangkul et al. [61] calculated the shift reaction equilibrium constant as follows:

$$K_{eq,shift} = \exp(-0.2935Z^3 + 0.6351Z^2 + 4.1788Z + 0.3169) \tag{99}$$

where

$$Z = \frac{1000}{T(K)} - 1 \tag{100}$$

However, equilibrium model is not a common assumption for refroming reaction in the papers.

3.4.5.2. Kinetic model. Some researchers claim that equilibrium cannot be assumed for the reforming reaction inside the solid oxide fuel cell due to a slow reforming kinetics compared with both shifting and hydrogen electrochemical oxidation. Therefore, the following general expression is used to evaluate the reforming rate and depends on reactants concentration and temperature.

$$r_{CH_4} = \lambda P_{CH_4}^m \cdot P_{H_2O}^n \exp\left(-\frac{E_a}{RT_{ct}}\right) \tag{101}$$

where E_a is the activation energy and λ is the pre-exponential factor.

Hajimolana and Soroush [22], Qi et al. [43], Nehter et al. [75] and Aguiar et al. [108] assumed a kinetic reforming reaction in their model.

3.5. Model equations for subsystem 5 (SS5)

This subsystem for TSOFC is the fuel that occupies and flows in the space on the anode side of the cell tube and for PSOFC is the fuel channel.

3.5.1. Mass transfer model

The multi-component mass transport in SOFC anodes is mainly coupled with the bulk chemical reactions, diffusion and convection of species while at the cathode side there is no chemical reaction. A total mass balance on the fuel and component mass balances on the fuel components for both TSOFC and PSOFC leads to:

$$\frac{\partial \rho^{ano}}{\partial t} + \nabla(u_{fuel}^{ano}\rho_{fuel}^{ano}) = \sum \nabla N_i \tag{102}$$

$$\frac{\partial \rho_{fuel}^{ano} Y_i}{\partial t} + \nabla(u_{fuel}^{ano}\rho_{fuel}^{ano} Y_i) = \nabla N_i + w_i \tag{103}$$

w_i is the rate of producing or consuming of components.

3.5.2. Heat transfer model

(i) An energy balance for the fuel gas inside SS5 for TSOFC results in:

$$\frac{\partial \rho_{fuel}^{ano} H_{fuel}^{ano}}{\partial t} = \nabla \Delta \rho_{fuel}^{ano} u_{fuel}^{ano} H_{fuel}^{ano} + Q^{ano} + Q_{diff}^{ano} + Q_{rad}^{ano} \tag{104}$$

In SS5, the convection heat transfer for TSOFC and PSOFC occurs between outside of the cell tube wall and the fuel flow inside the SS5 which is given by:

$$Q_{conv}^{ano} = h_{ct_o}(T_{ct_o} - T_{fuel}^{ano}) \tag{105}$$

Q_{rad}^{ano} in this subsystem for both TSOFC and PSOFC includes radiation heat transfer between walls and gas components. However, in most of the works, this type of radiation was neglected due to the lack of sufficiently accurate properties of gases.

Fuel components including H_2O, CH_4, CO, CO_2 and possibly other hydrocarbons are very strange spectral, temperature and pressure dependence and so can be treated as transparent [93].

This heat flow per wall unit area is evaluated by using Eq. (106) where the emissivity of the mixture of gases ε_g is calculated as proposed by Hadvig in [165], Eq. (107) and its absorptivity α_g as shown in Eq. (110) [166]. Subscripts w and g stands are for wall and gas in Eqs. (106)–(108) and i for the slice being analyzed.

$$q_{rad,i} = \frac{\varepsilon_w}{1-(1-\alpha_g)(1-\varepsilon_w)}\sigma(\varepsilon_g T_{gi}^4 - \alpha_g T_{w,i}^4) \tag{106}$$

$$\varepsilon_g = \varepsilon CO_2 - \varepsilon H_2O + \varepsilon CO_2 \varepsilon H_2O \tag{107}$$

$$\alpha_g = \varepsilon CO_2 \left(\frac{T_g}{T_w}\right)^{0.65} + \varepsilon H_2O \left(\frac{T_g}{T_w}\right)^{0.45} - \varepsilon CO_2 \varepsilon H_2O \tag{108}$$

Few studies considered radiation heat transfer between walls and gas components in their model [59].

(ii) An energy balance for the fuel gas inside SS5 for PSOFC results in:

$$\frac{\partial \rho_{fuel}^{ano} H_{fuel}^{ano}}{\partial t} = \nabla \Delta \rho_{fuel}^{ano} u_{fuel}^{ano} H_{fuel}^{ano} + Q^{ano} + Q_{diff}^{ano} + Q_{rad}^{ano} \tag{109}$$

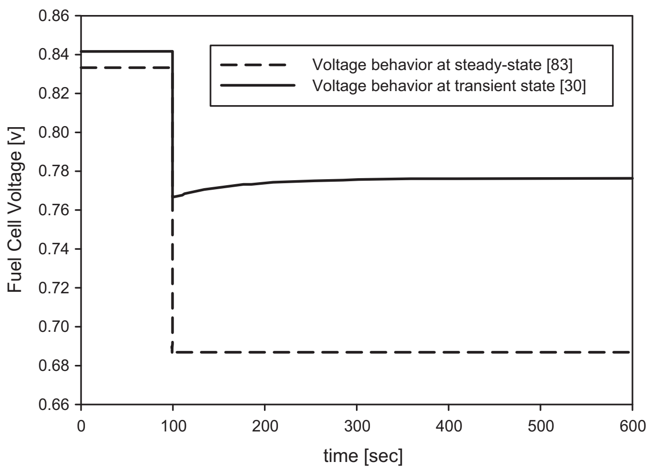


Fig. 5. The behavior of Fuel Cell Voltage at steady-state and transient condition.

In SS5, the convection heat transfer for PSOFC occurs between both the anode side of the cell tube wall and fuel side interconnector and the fuel flow inside the SS5 which is given by:

$$Q_{conv}^{ano} = h_{ct,a_o}(T_{ct,a_o} - T_{fuel}^{ch,a}) + h_{\text{int},a_i}(T^{ano} - T_{fuel}^{ch,a}) \quad (110)$$

The temperature distribution within the fuel cell is vital to SOFC operation, affecting the reaction kinetics and electrochemical model and these temperatures influence the voltage, polarization, heat generation within the cell, thus the overall cell performance. Based on the literatures, when only convection/conduction or convection/radiation heat transfer is considered large variations in cell temperature distribution and then in the cell performance was observed. In Fig. 6, there is a comparison between three different models regarding to distribution of cell temperature within the cell length. A complete heating components including radiation/convection/conduction/electrochemical and diffusional heating is involved in the T. Ota et al. [167] model, while R. Suwanwarangkul et al. [61] studied two different energy models, first a model including only conduction, convection and radiation and in the second model the radiation heat transfer is ignored. It is observed that the temperature difference between the minimum temperature and maximum temperature within the cell length is 87 K in T. Ota et al. [167] model 05 K and 145 in the first and second models of R. Suwanwarangkul et al. [61], respectively. Therefore, a strict temperature prediction distribution within SOFCs is essential for anticipating and optimizing the cell performances more accurately.

3.5.3. Momentum model

Momentum balance for the fuel in both TSOFC and PSOFC yields:

$$\frac{\partial(\rho_{fuel}^{ano} u_{fuel}^{ano})}{\partial t} + (\nabla \rho_{fuel}^{ano} u_{fuel}^{ano} u_{fuel}^{ano}) = \sum \nabla N_i M_i u_{fuel}^{ano} - \nabla P_{fuel}^{ano} + \nabla \tau_{fuel}^{ano} + F_{fuel}^{ano} \quad (111)$$

Pressure gradient in the anode and cathode side is important to the electrochemical activities of the fuel cell. It was found that by ignoring the anode pressure gradient in the model can make and error in calculating of concentration overpotential by about 20% at a current density and temperature of 5000 A m^{-2} and 1073 K, respectively [66].

3.5.3.1. Different fuels fed SOFCs. One of the most brightened advantages of solid oxide fuel cells over the other types of fuel cells is that hydrogen and carbon dioxide are used as fuel in the cell. This means that SOFC can use many common hydrocarbon fuels such as natural gas, diesel, gasoline and alcohol without the need to reform the fuel into pure hydrogen. In other fuel cells, such as the polymer electrolyte fuel cell, which are fueled with pure hydrogen, the carbon dioxide is a poison.

Hydrogen was considered as a fuel for SOFCs by Julian et al. [7], Wang et al. [126], Yuan et al. [168].

Hajimolana and Soroush [22], Autissier et al. [35], Aloui et al. [69], Aguiar et al. [108], Cui et al. [101], Janardhanan et al. [157], Fryda et al. [169] and Colpan et al. [170] considered hydrocarbon fuel fed to SOFCs.

Many authors like Suwanwarangkul et al. [61], Aloui et al. [69], Xie et al. [86] and other researchers in [61,69,86,171–179] tacked into account biomass as a fuel for SOFCs because it is abundant and renewable.

Hydrogen sulfide (H_2S) is a byproduct of natural gas which can also use as a fuel in the solid oxide fuel cells. There are two possible overall reactions that use H_2S directly in a SOFC:

$$H_2S + \frac{1}{2}O_2 \Leftrightarrow H_2O + \frac{1}{2}S_2 \quad (112)$$

$$H_2S + \frac{3}{2}O_2 \Leftrightarrow H_2O + SO_2 \quad (113)$$

However; it is not clear which of these reactions predominates in a SOFC running on H_2S.

Some researchers like Monder et al. [84], Liu et al. [163], Slavov et al. [164] and others in [84,163,164,180–185] used H_2S as a fuel in SOFCs.

Monder et al. [84] performed an isothermal steady state two-dimensional model of a planar SOFC fed by H_2S. In this paper, the performance of fuel cell fed by H_2S is not clear in comparison to other type of fuels.

Ahmed et al. [161] were the first group that compared the effect of different fuels on SOFC performance. A cross-flow monolithic solid oxide fuel cell honeycomb (MSOFC) structure with alternating layers of anode, electrolyte, cathode, and interconnect fed with different fuels, humidified hydrogen and coal gas, and air as oxidants was modeled. Results of the model with the simulated coal gas as the fuel and air as the oxidant showed that the MSOFC fed with coal gas reached a same cell voltage as a cell voltage of a hydrogen fed MSOFC but the coal gas MSOFC was expected a lower net power and a lower average current density.

Suwanwarangkul et al. [51], compared the performance of TSOFC using by biomass-derived synthesis gas as a fuel with the previous model (Suwanwarangkul et al. [61]) for a cell operating with humidified H_2. The results depicted that the cell performance for operating with humidified H_2 is more than that obtained with the synthesis gases because higher average temperatures within the cell were reached due to the higher energy content of humidified H_2. On the other hand, due to lower temperature distribution within the cell, the cell average temperature fed with synthesis gas is about 100 °C lower than that of humidified hydrogen.

Aloui et al. [69] presented an analytical modeling of polarization in a solid oxide fuel cell using biomass syngas product as fuel. The performance of fuel cell fed by biomass syngas was compared with the fuel cell fed by pure hydrogen. It was showed that a SOFC using the direct oxidation of syngas fuel (mixture of CO and H_2) is more powerful than that using only H_2 fuel.

Ni et al. [186] observed that the performance of CH_4 fed SOFC can promote at high operating temperature, as all the overpotentials decrease with increasing temperature. This behavior is different for H_2 fed SOFC performance, because by increasing the fuel cell temperature the concentration overpotential also increases.

P. Dokmaingam et al. [77], performed a mathematical two-dimensional steady state model of an indirect internal reforming tubular solid oxide fuel cell fed by four different primary fuels, i.e.,

methane, biogas, methanol and ethanol. The objective of this paper was to investigate the effect of fuel type on the thermal coupling between internal endothermic reforming with exothermic electrochemical reactions and system performance. It was observed that indirect internal reforming SOFC fed by methanol has the greatest performance in terms of electrical efficiency and temperature distribution along the system. Based on this study, CO_2 in biogas affects the system performance significantly. The electrical efficiency can be improved by removal of some carbon monoxide from biogas; however, a greater temperature gradient is expected.

Brett et al. [187] were interested in studying on methanol fed SOFCs with an intermediate range of temperature between 500 and 600 °C. A lower operating temperature induces a more rapid start-up and shut-down, decreases the cell temperature fluctuation and then thermal stress in the ceramics. In addition, at a low operating temperature the dimensional thickness of the electrolyte can be reduced, giving almost the same results by promoting the ionic conductivity of the electrolyte at lower operating temperatures [159]. Moreover, fueling an SOFC directly by methanol ignores the internal reforming process with large thermal gradients within the fuel cell.

Arpornwichanop et al. [188] studied the performance of an anode-supported SOFC fed by ethanol under a direct internal reforming and isothermal condition. Electrochemical mode including all polarization losses was investigated in details. It was illustrated that cell temperature, the ratio of steam to ethanol and the inlet feed flow substantially affect the electrical efficiency of SOFC. In this study, the performance of fuel cell fed by ethanol was not compared with other fuels fed solid oxide fuel cell.

4. Literature on the SOFC configuration

Tubular and planer solid oxide fuel cells are discussed generally in Section 2. These two types of SOFCs are common configurations used in the literatures. Some researchers were interested in modeling both T-SOFC and P-SOFC. Ferguson et al. [50], studied a three-dimensional mathematical model on both tubular and planner SOFCs with considering a local distribution of the electrical potential, temperature and concentration of the chemical species inside the both configurations. By comparing both tubular and planar solid oxide fuel cells a less ohmic loss and higher efficiency for the former geometry was observed.

Stiller et al. [28] like Ferguson's group [50] were interested in both planar and tubular solid oxide fuel cells modeling. However; the study was focused more on effects of parameters on both fuel cell configurations with a 2D steady-state planar and tubular SOFCs fed by methane. The model was involved of ohmic resistance, convective, conductive and radiation heat transfers, chemical reactions and mass conservations. The required boundary conditions and input parameters of the models were discussed. The objective of the study was to observe the impact of inlet air flow temperature, pressure ratio, air flow rate and anode gas recycling on both configurations. It was illustrated that the cycle balance is different in both systems, as the tubular fuel cell required a lower air inlet temperature. Both fuel cell systems achieved above 65% electric efficiency.

A complete comparison between tubular and planar solid oxide fuel cell configurations was presented by Zhang et al. [156]. A three-dimensional steady-state numerical model for both configurations was described. This paper conducted detailed analyses of the electric polarizations for both configurations and presented the characteristics of the potential distribution in the electric components for the planar co-flow SOFC. The results were in a good agreement with the experimental data. Based on the results, for planar SOFC, polarizations results in the electrolyte ohmic loss and the activation polarization but for the tubular SOFC, the cathode ohmic loss has the greatest contribution to the sum of polarizations while the activation polarization is the next highest loss. It was also shown that the ohmic heat predominately depends on the current density in the planar SOFC while in tubular configuration the ohmic heat is produced from the cathode. The relative ohmic heat contribution to the total heat is higher for the tubular than for the planar configuration, and for the planar SOFC, this is more pronounced in the counter-flow design than in the co-flow design. Before Zhang et al. group [156] the effect of different flow manifolding, i.e., cross-co, or counter-flow were considered by Achenbach [116]. It was showed that the highest fuel cell efficiency is obtained for counter-flow, the most uniform current density distribution is reached for co-flow and the largest temperature gradients in the solid structure occur for cross-flow. Ferguson et al. [50] compared the counter flow and co-flow for planar geometry in their model and revealed that the counter flow for hydrogen as a fuel is the most suitable flow configuration. A comparison between counter-flow and co-flow was performed by Aguiar et al. [108]. It was presented that for the counter-flow configuration the temperature increases along the air flow direction with the maximum at the outlet and for the co-flow configuration the temperature profile reaches to its maximum value near the fuel flow outlet. In this system co-flow configuration is the more efficient one due to the high air temperature.

5. Novel SOFC models

As a kind of nonlinear multi-input–multi-output (MIMO) system, SOFC is hard to model by the traditional methodologies. Therefore; some researchers have attempted to establish novel fuel cell models by statistical data-driven approach. Data-driven approach is based on analyzing the data about a system, in particular finding relationships between the input and output variables of the system without explicit knowledge of its physical behavior. The artificial neural network model is a novel model which is very useful for rapid calculation of SOFC e.g. dynamic, static and control simulations. The Hammerstein models is also a novel method for modeling SOFCs which include a nonlinear block followed by the linear system and are useful to model static and dynamic systems of the solid oxide fuel cell.

Some researchers have attempted to establish novel SOFC models [189,190,194–196].

Jurado [149] developed a multivariable Hammerstein model of a SOFC, which is applicable for small signal and dynamic stability studies. The Hammerstein models include a nonlinear block followed by the linear system and are useful to model static and dynamic systems of the solid oxide fuel cell. Dynamic behavior of temperature and output voltage losses was explained by considering the electrochemical and thermal equations in this paper. Non-iterative algorithms for the identification of multivariable Hammerstein system were studied. The main debate in the derivation of the results was the representation of the system using base functions.

Bo Huo et al. [191] reported a dynamic modeling of SOFC using Hammerstein Model for dynamic simulation and control. The static nonlinear of the Hammerstein model was modeled by a radial basis function neural network (RBFNN), and the linear part was modeled by an autoregressive with exogenous input (ARX) model. In this study, a new gradient descent algorithm was used to anticipate the hidden centers, the radial basis function widths and the connection weights of the RBFNN. For anticipating the parameters and the orders of the ARX model, the least squares (LS) algorithm and Akaike Information Criteria (AIC) were derived, respectively. By comparing the Hammerstein model and the RBFNN model exper-

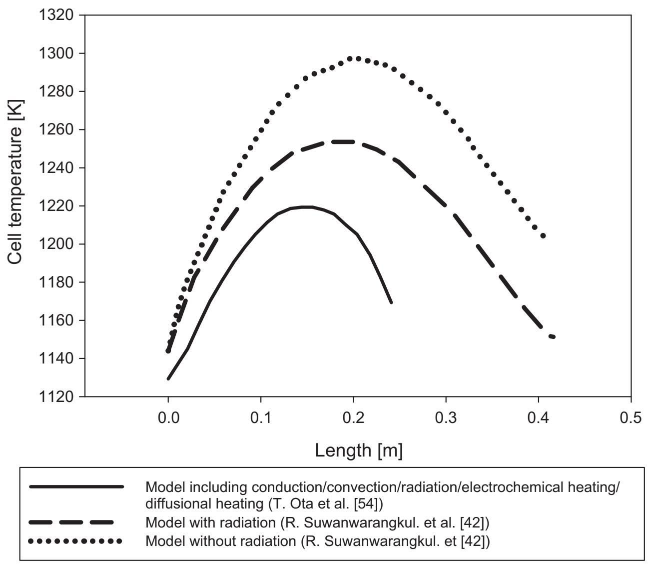


Fig. 6. Comparison of cell temperature distribution between three different models.

imentally, a better performance for the Hammerstein model was reported in this study.

Wu et al. [192] presented a nonlinear offline model of SOFC used a radial basis function neural network based on genetic algorithm. The objective of the work was to optimize the parameters of radial basis function neural networks. The model was validated by the simulations. The simulation results illustrated that radial basis function neural network based on genetic algorithm method is superior to the conventional back progration neural network in predicting the stack voltage with different temperature basis parameter neural network in anticipating the fuel cell voltage in case of different temperature. Although many other operating parameters are also effective on fuel cell performance, only current density and temperature was considered in this model. Wu group [193] also studied the different flows effect on the performance of SOFC by developing an adaptive neural-fuzzy inference system (ANFIS). In order to identify linear and nonlinear parameters in the ANFIS, a hybrid learning algorithm combining back propagation and least squares estimate was adopted. The results were compared by simulations and the simulation results showed that the ANFIS model can efficiency predict the dynamic behavior of SOFC. However, the model was not included the temperature dynamic response and the SOFC fuel processor was also not considered.

Milewski et al. [190] found that the Artificial Neural Network can be used to simulate the fuel cell behavior only by utilizing available experimental data. The cell voltage was predicted by the inputs of the model which were current density, temperature, fuel volume flow density, and oxidant volume flow density. The results reveal that the ANN can be efficiently used for the single SOFC with relatively high accuracy. Table 7 shows some researchers that focused on novel models.

6. Conclusion

Mathematical modeling is an essential tool in design of fuel cell systems, as it is important to understand the response of a cell stack under normal or transient conditions. Such models can provide a picture of cell stress, potential, current density, and temperature as functions of position and time for various cell configurations and operating conditions, and be used to examine the effects of changes on one or more variables and the relative system sensitivity to relevant design parameters. A model is also useful in predicting the effects of altering process variables and in using that information to optimize cell performance. Many research studies have been done in this regard. However, still many aspects of fuel cell modeling are remained for studying (Fig. 6).

In this study, mathematical modeling of SOFCs for both tubular and planar configurations was reviewed into five subsystems considering the factors like polarization losses, mass/energy/momentum conservations, diffusion through porous media, and electrochemical phenomena in the PEN region and shift/reforming reactions inside them which is novel in this regard. Also, using variety of fuels fed to the SOFCs was discussed and their effect on the system was compared briefly. A short review of solid oxide fuel cell configurations and different flow manifolding were also presented in this review study. For the first time in this area, novel models based on statistical data-driven approach existing in the literatures were studied.

In this section we point to the subjects that need further research.

Fuel cell temperature and voltage strikingly depend on electrochemical reaction. The electrochemical oxidation of both hydrogen and carbon monoxide occurs on the triple phase boundary, whereas the proportion of these two reactions is still unknown. CO oxidation influences the overall performance of the cell and on the other hand, polarization resistances impress voltage directly. In many studies CO oxidation at electrochemical reaction is neglected or polarization losses are not completely accounted. However, it is not still quite clear that by making some simplified assumptions for the electrochemical modeling how they can influence the accuracy of the model. What the difference between observed experimental values and the results of the mathematical modeling is. Calculating the errors even for small changes means that there is something we do not understand and need to account for it. Therefore, such phenomena should be deeply studied in both mathematical modeling and experimentation fields to perform a more accurate and validated model.

Very limited studies focused on how the SOFC microstructure influence the chemical reactions and mass transfer in the porous SOFC electrode. Generally, length of TPB, porosity, particle size and thicknesses of electrodes and electrolytes has conflicting effect on the PEN performance. Thus, optimal design for PEN in order to improve the PEN efficiency is significant.

Diffusion through porous media significantly affects the performance of solid oxide fuel cells. Fuel cell voltage and polarization losses depend on the concentration of components inside the triple phase boundary. In addition, diffusional heat transfer influences the fuel cell temperature. Therefore, it is necessary to consider diffusion in models in order to have an accurate prediction of fuel cell behaviors. Although several research has been done for presenting a beneficial diffusional model (FM, SMM, DGM) at different conditions, still more investigation requires to compare these three models together to minimize the error between mathematical modeling and experimental results.

Among the papers which were studied in this work, was shown that some of the models ignored radiative heat transfer between free walls and especial between gas components. Many works accounted radiation heat transfer in their model but the knowledge of thermal radiation property for both bulk and surface properties at high temperatures relevant to SOFC is still incomplete and requires more study in this regard.

Electrochemical heating is also still not fully available in open literature and is imperative to develop in the models. Ohmic heating must be tacked into account in SOFC models due to the large ionic resistance of YSZ compared to heat of electrolyte materials used in other types of fuel cells. Moreover, conduction heat transfer in many papers was neglected while accurate determination of the temperature distribution including the radiation, conduction, diffusional heat transfer and electrochemical heating is required since

the material properties, chemical kinetics, and transport properties of materials used in single cell and stack level depends on the temperature.

Neglecting the momentum balance by several researchers was not fully justified. More research studies require showing the effect of momentum balance especially inside the porous electrodes on solid oxide fuel cell performance.

The pressure gradient in the electrodes of SOFCs is simply ignored without any justification in modeling studies. Therefore the effect of pressure distribution on mass transfer and thus on overpotential should be more studied.

A major advantage of solid oxide fuel cells over other types of fuel cells is that a variety of hydrocarbon-based gases or their synthesis derivatives, such as natural gas, biomass and coal can potentially be used as fuel sources. It was shown that a SOFC using the direct oxidation of syngas fuel (mixture of CO and H_2) is more powerful than using pure H_2 fuel, and also methanol in comparison to other fuels like methane, biogas, and ethanol as fuels, has the greatest performance in terms of electrical efficiency. However, still a complete research study needs to present a suitable fuel for promoting the SOFCs performance and their power efficiency. In addition, the effect of each fuel on the important factors of SOFCs such as cell temperature, voltage, reactions, and cell performance is not completely studied.

In many papers the effect of reformers and different geometries and configurations is not clear. It is imperative to show the importance of the mentioned factors in the models.

The intelligent novel models avoid the complexity of the mathematical model and provide the input-output relationship much faster and easier. Based on these models, valid control strategy studies like predictive control and robust control can be developed. Therefore, more research studies requires for developing the novel models.

References

[1] Sopian K, Wan Daud WR. Challenges and future developments in proton exchange membrane fuel cells. Renewable and Sustainable Energy 2006;31:719–27.

[2] Sopian K, Shamsuddin AH, Nejat Veziroglu T. Solar hydrogen energy option for Malaysia. In: Proceeding of the international conference on advances in strategic technology. 1995. p. 209–29.

[3] Ramakumar R, Chiradeja P. Distributed generation and renewable energy systems. In: Proceedings of the 37th intersociety energy conversion engineering conference. 2002. p. 716–24.

[4] Caisheng W, Hashem N. Distributed generation applications of fuel cells. In: Power systems conference: advanced metering, protection, control communication and distributed resources. 2006. p. 244–8.

[5] Boudghene S, Traversa E. An alternative to standard sources of energy. Renewable and Sustainable Energy Reviews 2002:297–306.

[6] Stambouli AB, Traversa E. Solid oxide fuel cells (SOFCs): a review of an environmentally clean and efficient source of energy. Renewable and Sustainable Energy Reviews 2002;6:433–55.

[7] Julian M. A distributed power generation communication system. In: Proceedings of the IEEE Canadian conference on electronic computer engineering. 2003. p. 483–539.

[8] Badwal SPS, Foger K. Solid oxide electrolyte fuel cell review. Ceramics International 1996;22:257–65.

[9] Zhu WZ, Deevi Sc. A review on the status of anode materials for solid oxide fuel cells. Materials Science and Engineering A 2003;362:228–39.

[10] Qiu-An Huang RH, Bingwen Wang, Jiujun Zhang. A review of AC impedance modeling and validation in SOFC diagnosis. Electrochimica Acta 2007;52:8144–64.

[11] Zhang X, Chan SH, Li G, Ho HK, Li J, Feng Z. A review of integration strategies for solid oxide fuel cells. Journal of Power Sources 2010;195:685–702.

[12] Bhattacharyya D, Rengaswamy R. A review of solid oxide fuel cell (SOFC) dynamic models. Industrial & Engineering Chemistry 2009;48:6068–86.

[13] Kakaç S, Pramuanjaroenkij A, Zhou XY. A review of numerical modeling of solid oxide fuel cells. International Journal of Hydrogen Energy 2007;32:761–86.

[14] Lawlor V, Griesser S, Buchinger G, Olabi AG, Cordiner S, Meissner D. Review of the micro-tubular solid oxide fuel cell: Part I. Stack design issues and research activities. Journal of Power Sources 2009;193:387–99.

[15] Lawlor V, Griesser S, Buchinger G, Olabi AG, Cordiner S, Meissner D. Review of the micro-tubular solid oxide fuel cell: Part I. Stack design issues and research activities. Journal of Power Sources 2009;195:936–1036.

[16] Andersson M, Yuan J, Sundén B. Review on modeling development for multiscale chemical reactions coupled transport phenomena in solid oxide fuel cells. Applied Energy 2010;87:1461–76.

[17] Bavarian M, Soroush M, Kevrekidis IG, Benziger JB. Mathematical modeling, steady-state and dynamic behavior, and control of fuel cells: a review. Industrial & Engineering Chemistry Research 2010.

[18] O'hayre RBDM, Prinz FB. The triple phase boundary a mathematical model and experimental investigations for fuel cells. Electrochemistry 2005;152:439–44.

[19] Farooque M, Maru H. Fuel cells—the clean and efficient power generators. IEEE Proceedings 2001;89:1819–29.

[20] Swider-Lyons Ke CR, Rosenfeld RL, Nowak RJ. Technical issues and opportunities for fuel cell development for autonomous underwater vehicles. In: Proceedings of workshop on autonomous underwater vehicle. 2002. p. 61–4.

[21] Yakabe H, Sakuri T, Sobue T, Yamashita S, Hase K. Solid oxide fuel cells as promising candidates for distributed generators. IEEE International Conference on Industrial Information 2006:369–74.

[22] Hajimolana S Ahmad, Soroush M. Dynamics and control of a tubular solid-oxide fuel cell. Industrial & Engineering Chemistry 2009;48:6112–25.

[23] Holtappels P, De Haart L, Stimming U, Vinke I, Mogensen M. Reaction of CO/CO_2 gas mixtures on Ni–YSZ cermet electrodes. Applied Electrochemistry 1999;29:561–8.

[24] Matzusaki Y, Hishinuma M, Yasuda I. Proceedings of solid oxide fuel cell. The Electrochemical Society Proceedings Series 1999;5:560–6.

[25] Mahcene H, Moussa HB, Bouguettaia H, Bechki D, Babay S, Meftah Ms. Study of species, temperature distributions and the solid oxide fuel cells performance in a 2-D model. International Journal of Hydrogen Energy, in press.

[26] Costamagna P, Costa P, Antonucci V. Micro-modelling of solid oxide fuel cell electrodes. Electrochimica Acta 1998;43:375–94.

[27] Burt AC, Celik IB, Gemmen RS, Smirnov AV. A numerical study of cell-to-cell variations in a SOFC stack. Journal of Power Sources 2004;126:76–87.

[28] Stiller C, Thorud B, Seljebø S, Mathisen Ø, Karoliussen H, Bolland O. Finite-volume modeling and hybrid-cycle performance of planar and tubular solid oxide fuel cells. Journal of Power Sources 2005;141:227–40.

[29] Ji Y, Yuan K, Chung JN, Chen Y-C. Effects of transport scale on heat/mass transfer and performance optimization for solid oxide fuel cells. Journal of Power Sources 2006;161:380–91.

[30] Chan SH, Khor KA, Xia Zt. A complete polarization model of a solid oxide fuel cell and its sensitivity to the change of cell component thickness. Journal of Power Sources 2001;93:130–40.

[31] Yakabe H, Ogiwara T, Hishinuma M, Yasuda I. 3-D model calculation for planar Sofc. Journal of Power Sources 2001;102:144–54.

[32] Bove R, Ubertini S. Modeling solid oxide fuel cell operation: approaches, techniques and results. Journal of Power Sources 2006;159:543–59.

[33] Ho TX, Kosinski P, Hoffmann AC, Vik A. Modeling of transport, chemical and electrochemical phenomena in a cathode-supported SOFC. Chemical Engineering Science 2009;64:3000–9.

[34] Qi Y, Huang B, Chuang Kt. Dynamic modeling of solid oxide fuel cell: the effect of diffusion and inherent impedance. Journal of Power Sources 2005;150:32–47.

[35] Autissier N, Larrain D, Van Herle J, Favrat D. CFD simulation tool for solid oxide fuel cells. Journal of Power Sources 2004;131:313–9.

[36] Hussain MM, Li X, Dincer I. A numerical investigation of modeling an SOFC electrode as two finite layers. International Journal of Hydrogen Energy 2009;34:3134–44.

[37] Hussain MM, Li X, Dincer I. A general electrolyte-electrode-assembly model for the performance characteristics of planar anode-supported solid oxide fuel cells. Journal of Power Sources 2009;189:916–28.

[38] Izzo Jr JR, Peracchio AA, Chiu WKS. Modeling of gas transport through a tubular solid oxide fuel cell and the porous anode layer. Journal of Power Sources 2008;176:200–6.

[39] Chaisantikulwat A, Diaz-Goano C, Meadows ES. Dynamic modelling and control of planar anode-supported solid oxide fuel cell. Computers & Chemical Engineering 2008;32:2365–81.

[40] Cayan FN, Pakalapati SR, Elizalde-Blancas F, Celik I. On modeling multi-component diffusion inside the porous anode of solid oxide fuel cells using Fick's model. Journal of Power Sources 2009;192:467–74.

[41] Ni M, Leung Dyc, Leung Mkh. Electrochemical modeling and parametric study of methane fed solid oxide fuel cells. Energy Conversion and Management 2009;50:268–78.

[42] Yakabe H, Hishinuma M, Uratani M, Matsuzaki Y, Yasuda I. Evaluation and modeling of performance of anode-supported solid oxide fuel cell. Journal of Power Sources 2000;86:423–31.

[43] Qi Y, Huang B, Luo J. Dynamic modeling of a finite volume of solid oxide fuel cell: the effect of transport dynamics. Chemical Engineering Science 2006;61:6057–76.

[44] Nagata S, Momma A, Kato T, Kasuga Y. Numerical analysis of output characteristics of tubular SOFC with internal reformer. Journal of Power Sources 2001;101:60–71.

[45] Ho TX, Kosinski P, Hoffmann AC, Vik A. Numerical modeling of solid oxide fuel cells. Chemical Engineering Science 2008;63:5356–65.
[46] Ho TX, Kosinski P, Hoffmann AC, Vik A. Numerical analysis of a planar anode-supported SOFC with composite electrodes. International Journal of Hydrogen Energy 2009;34:3488–99.
[47] Ni M, Leung DYC, Leung MKH. Importance of pressure gradient in solid oxide fuel cell electrodes for modeling study. Journal of Power Sources 2008;183:668–73.
[48] Nikooyeh K, Jeje AA, Hill JM. 3D modeling of anode-supported planar SOFC with internal reforming of methane. Journal of Power Sources 2007;171:601–9.
[49] Morel B, Laurencin J, Bultel Y, Lefebvre-Joud F. Anode-supported sofc model centered on the direct internal reforming. Journal of the Electrochemical Society 2005;152:1382–9.
[50] Ferguson JR, Fiard JM, Herbin R. Three-dimensional numerical simulation for various geometries of solid oxide fuel cells. Journal of Power Sources 1996;58:109–22.
[51] Suwanwarangkul R, Croiset E, Pritzker MD, Fowler MW, Douglas PL, Entchev E. Modelling of a cathode-supported tubular solid oxide fuel cell operating with biomass-derived synthesis gas. Journal of Power Sources 2007;166:386–99.
[52] Suwanwarangkul R, Croiset E, Fowler MW, Douglas PL, Entchev E, Douglas MA. Performance comparison of Fick's, dusty-gas and Stefan-Maxwell models to predict the concentration overpotential of a SOFC anode. Journal of Power Sources 2003;122:9–18.
[53] Karcz M. From 0D to 1D modeling of tubular solid oxide fuel cell. Energy Conversion and Management 2009;50:2307–15.
[54] Bhattacharyya D, Rengaswamy R, Finnerty C. Isothermal models for anode-supported tubular solid oxide fuel cells. Chemical Engineering Science 2007;62:4250–67.
[55] Virkar AV. Low-temperature anode-supported high power density solid oxide fuel cells with nano-structured electrodes. University of Utah; 2000.
[56] Kim JW, Virkar AV, Fung KZ, Mentha K, Singhal SC. Polarization effects in intermediate temperature, anode-supported solid oxide fuel cells. Electrochemical Society 1999;146:69–78.
[57] Bove R, Lunghi P, Sammes NM. SOFC mathematic model for systems simulations. Part one: from a micro-detailed to macro-black-box model. International Journal of Hydrogen Energy 2005;30:181–7.
[58] Sánchez D, Muñoz A, Sánchez T. An assessment on convective and radiative heat transfer modelling in tubular solid oxide fuel cells. Journal of Power Sources 2007;169:25–34.
[59] Sánchez D, Chacartegui R, Muñoz A, Sánchez T. On the effect of methane internal reforming modelling in solid oxide fuel cells. International Journal of Hydrogen Energy 2008;33:1834–44.
[60] Jin X, Xue X. Mathematical modeling analysis of regenerative solid oxide fuel cells in switching mode conditions. Journal of Power Sources 2010;195:6652–8.
[61] Suwanwarangkul R, Croiset E, Pritzker MD, Fowler MW, Douglas PL, Entchev E. Mechanistic modelling of a cathode-supported tubular solid oxide fuel cell. Journal of Power Sources 2006;154:74–85.
[62] Zhu H, Kee Rj. A general mathematical model for analyzing the performance of fuel-cell membrane-electrode assemblies. Journal of Power Sources 2003;117:61–74.
[63] Jeon DH. A comprehensive CFD model of anode-supported solid oxide fuel cells. Electrochimica Acta 2009;54:2727–36.
[64] Nam JH, Jeon DH. A comprehensive micro-scale model for transport and reaction in intermediate temperature solid oxide fuel cells. Electrochimica Acta 2006;51:3446–60.
[65] Lehnert W, Meusinger J, Thom F. Modelling of gas transport phenomena in SOFC anodes. Journal of Power Sources 2000;87:57–63.
[66] Ni M, Leung DYC, Leung MKH. Mathematical modeling of ammonia-fed solid oxide fuel cells with different electrolytes. International Journal of Hydrogen Energy 2008;33:5765–72.
[67] Janardhanan VM, Deutschmann O. Numerical study of mass and heat transport in solid-oxide fuel cells running on humidified methane. Chemical Engineering Science 2007;62:5473–86.
[68] Suwanwarangkul R, Croiset E, Entchev E, et al. Experimental and modeling study of solid oxide fuel cell operating with syngas fuel. Journal of Power Sources 2006;161:308–22.
[69] Aloui T, Halouani K. Analytical modeling of polarizations in a solid oxide fuel cell using biomass syngas product as fuel. Applied Thermal Engineering 2007;27:731–7.
[70] Chen D, Bi W, Kong W, Lin Z. Combined micro-scale and macro-scale modeling of the composite electrode of a solid oxide fuel cell. Journal of Power Sources 2010;195:6598–610.
[71] Tsai C-L, Schmidt VH. Tortuosity in anode-supported proton conductive solid oxide fuel cell found from current flow rates and dusty-gas model. Journal of Power Sources 2011;196:692–9.
[72] Tseronis K, Kookos IK, Theodoropoulos C. Modelling mass transport in solid oxide fuel cell anodes: a case for a multidimensional dusty gas-based model. Chemical Engineering Science 2008;63:5626–38.
[73] Geankoplis CJ. Mass transport phenomena. New York: Holt, Rinehart & Winston; 1972.
[74] Arpino F, Massarotti N. Numerical simulation of mass and energy transport phenomena in solid oxide fuel cells. Energy 2009;34:2033–41.
[75] Nehter P. Two-dimensional transient model of a cascaded micro-tubular solid oxide fuel cell fed with methane. Journal of Power Sources 2006;157:325–34.
[76] Bhattacharyya D, Rengaswamy R, Finnerty C. Dynamic modeling and validation studies of a tubular solid oxide fuel cell. Chemical Engineering Science 2009;64:2158–72.
[77] Dokamaingam P, Assabumrungrat S, Soottitantawat A, Laosiripojana N. Effect of operating conditions and gas flow patterns on the system performances of IIR-SOFC fueled by methanol. International Journal of Hydrogen Energy 2009;34:6415–24.
[78] Dokamaingam P, Assabumrungrat S, Soottitantawat A, Sramala I, Laosiripojana N. Modeling of SOFC with indirect internal reforming operation: comparison of conventional packed-bed and catalytic coated-wall internal reformer. International Journal of Hydrogen Energy 2009;34:410–21.
[79] Qu Z, Aravind PV, Dekker NJJ, Janssen AHH, Woudstra N, Verkooijen AHM. Three-dimensional thermo-fluid and electrochemical modeling of anode-supported planar solid oxide fuel cell. Journal of Power Sources 2003;195:7787–95.
[80] Welty Jrw, Wilson CE, Rorrer Re. Fundamentals of momentum, heat, and mass transfer. 4th Edition. New York: Wiley; 2000.
[81] Perry RGD, Maloney J. Perry's chemical engineers' handbook. 7th ed. McGraw-Hill; 1997.
[82] El C. Diffusion mass transfer in fluid systems. Cambridge University Press; 1997.
[83] Xue X, Tang J, Sammes N, Du Y. Dynamic modeling of single tubular SOFC combining heat/mass transfer and electrochemical reaction effects. Journal of Power Sources 2005;142:211–22.
[84] Monder DS, Nandakumar K, Chuang KT. Model development for a SOFC button cell using H_2S as fuel. Journal of Power Sources 2006;162:400–14.
[85] Shi Y, Cai N, Li C, Bao C, Croiset E. Modeling of an anode-supported Ni–YSZ|Ni–ScSZ|ScSZ|LSM–ScSZ multiple layers SOFC cell Part I. Experiments, model development and validation. Journal of Power Sources 2007;172:235–45.
[86] Xie Y, Xue X. Transient modeling of anode-supported solid oxide fuel cells. International Journal of Hydrogen Energy 2009;34:6882–91.
[87] Martinez AS, Brouwer J. Modeling and comparison to literature data of composite solid oxide fuel cell electrode-electrolyte interface conductivity. Journal of Power Sources 195; 7268–77.
[88] Hayes RE, Kolaczkowski ST. Introduction to catalytic combustion. Amsterdam: Gordon and Breach Science Publishers; 1997.
[89] Damm DL, Fedorov AG. Reduced-order transient thermal modeling for SOFC heating and cooling. Journal of Power Sources 2006;159:956–67.
[90] Klein JM, Bultel Y, Georges S, Pons M. Modeling of a SOFC fuelled by methane: from direct internal reforming to gradual internal reforming. Chemical Engineering Science 2007;62:1636–49.
[91] Iora P, Aguiar P, Adjimanb CS, Brandon NP. Comparison of two IT DIR-SOFC models: impact of variable thermodynamic, physical, and flow properties. Steady-state and dynamic analysis. Chemical Engineering Science 2005;60:2963–75.
[92] Colclasure AM, Sanandaji BM, Vincent TL, Kee Rj. Modeling and control of tubular solid-oxide fuel cell systems. I: Physical models and linear model reduction. Journal of Power Sources 2010;196:196–207.
[93] Modest MF. Radiative heat transfer. 2nd ed. New York: Academic Press; 2003.
[94] Mauri R. A new application of the reciprocity relations to the study of fluid flows through fixed beds. Engineering Mathematics 1998;33:103–12.
[95] Song TW, Sohn JL, Kim JH, Kim TS, Ro ST, Suzuki K. Performance analysis of a tubular solid oxide fuel cell/micro gas turbine hybrid power system based on a quasi-two dimensional model. Journal of Power Sources 2005;142: 30–42.
[96] Kandepu R, Imsland L, Foss BA, Stiller C, Thorud B, Bolland O. Modeling and control of a SOFC-GT-based autonomous power system. Energy 2007;32:406–17.
[97] Kang Y, Li J, Cao G, Tu H, Li J, Yang J. One-dimensional dynamic modeling and simulation of a planar direct internal reforming solid oxide fuel cell. Chinese Journal of Chemical Engineering 2009;17:304–17.
[98] Wang L, Zhang H, Weng S. Modeling and simulation of solid oxide fuel cell based on the volume–resistance characteristic modeling technique. Journal of Power Sources 2008;177:579–89.
[99] Danilov VA, Tade MO. A CFD-based model of a planar SOFC for anode flow field design. International Journal of Hydrogen Energy 2009;34:8998–9006.
[100] Li PW, Chyu MK. Simulation of the chemical/electrochemical reactions and heat/mass transfer for a tubular SOFC in a stack. Journal of Power Sources 2003;124:487–98.
[101] Cui D, Liu L, Dong Y, Cheng M. Comparison of different current collecting modes of anode supported micro-tubular SOFC through mathematical modeling. Journal of Power Sources 2007;174:246–54.
[102] Haberman BA, Young JB. Three-dimensional simulation of chemically reacting gas flows in the porous support structure of an integrated-planar solid oxide fuel cell. International Journal of Heat and Mass Transfer 2004;47:3617–29.
[103] Ni M. 2D thermal-fluid modeling and parametric analysis of a planar solid oxide fuel cell. Energy Conversion and Management 2010;51:714–21.
[104] Young DF, Munson BR, Okiishi TH. A brief introduction to fluid mechanics. New York, Chichester, Brisbane, Toronto, Singapore, Weinheim: Wiley; 1996.
[105] Tien HC, Chiang KC. Non-Darcy flow and heat transfer in a porous insulation with infiltration and natural convection. Marine Science & Technology 1999;7:125–31.
[106] Doraswami U, Droushiotis N, Kelsall GH. Modelling effects of current distributions on performance of micro-tubular hollow fibre solid oxide fuel cells. Electrochimica Acta 2010;55:3766–78.

[107] Vogler M, Horiuchi M, Bessler WG. Modeling, simulation and optimization of a no-chamber solid oxide fuel cell operated with a flat-flame burner. Journal of Power Sources 195:7067–77.
[108] Aguiar P, Chadwick D, Kershenbaum L. Modelling of an indirect internal reforming solid oxide fuel cell. Chemical Engineering Science 2002;57:1665–77.
[109] Aguiar P, Adjiman CS, Brandon NP. Anode-supported intermediate-temperature direct internal reforming solid oxide fuel cell: II. Model-based dynamic performance and control. Journal of Power Sources 2005;147:136–47.
[110] Aguiar P, Adjiman CS, Brandon NP. Anode-supported intermediate temperature direct internal reforming solid oxide fuel cell. I: model-based steady-state performance. Journal of Power Sources 2004;138:120–36.
[111] Murshed AM, Huang B, Nandakumar K. Control relevant modeling of planer solid oxide fuel cell system. Journal of Power Sources 2007;163: 830–45.
[112] Nagel FP, Schildhauer TJ, Biollaz Sma, Stucki S. Charge, mass and heat transfer interactions in solid oxide fuel cells operated with different fuel gases—a sensitivity analysis. Journal of Power Sources 2008;184:129–42.
[113] Nagel FP, Schildhauer TJ, Biollaz Sma, Wokaun A. Performance comparison of planar, tubular and Delta8 solid oxide fuel cells using a generalized finite volume model. Journal of Power Sources 2008;184:143–64.
[114] Cheddie DF, Munroe NDH. A dynamic 1D model of a solid oxide fuel cell for real time simulation. Journal of Power Sources 2007;171:634–43.
[115] Jia J, Abudula A, Wei L, Jiang R, Shen S. A mathematical model of a tubular solid oxide fuel cell with specified combustion zone. Journal of Power Sources 2007;171:696–705.
[116] Achenbach E. Three-dimensional and time-dependent simulation of a planar solid oxide fuel cell stack. Journal of Power Sources 1994;49:333–48.
[117] Bessette NF, Wepfer WJ. Prediction of on-design and off-design performance for a solid oxide fuel cell power module. Energy Conversion and Management 1996;37:281–93.
[118] Costamagna P, Selimovic A, Del Borghi M, Agnew G. Electrochemical model of the integrated planar solid oxide fuel cell (IP-SOFC). Chemical Engineering Journal 2004;102:61–9.
[119] Achenbach E, Riensche E. Methane/steam reforming kinetics for solid oxide fuel cells. Journal of Power Sources 1994;52:283–8.
[120] Salogni A. P. C. Modeling of solid oxide fuel cells for dynamic simulations of integrated systems. Applied Thermal Engineering 2009;30:464–77.
[121] Brus G, Szmyd JS. Numerical modelling of radiative heat transfer in an internal indirect reforming-type SOFC. Journal of Power Sources 2008;181: 8–16.
[122] Calise F, Dentice D'accadia M, Restuccia G. Simulation of a tubular solid oxide fuel cell through finite volume analysis: Effects of the radiative heat transfer and exergy analysis. International Journal of Hydrogen Energy 2007;32:4575–90.
[123] Haynes C. Simulating process settings for unslaved SOFC response to increases in load demand. Journal of Power Sources 2002;109:365–76.
[124] Ma Z. A combined differential and integral model for high temperature fuel cells. PhD Thesis. Georgia: Georgia Institute of Technology; 2000.
[125] Iwai H, Yamamoto Y, Saito M, Yoshida H. Numerical simulation of intermediate-temperature direct-internal-reforming planar solid oxide fuel cell. Energy 2010:1–10.
[126] Wang G, Yang Y, Zhang H, Xia W. 3-D model of thermo-fluid and electrochemical for planar Sofc. Journal of Power Sources 2007;167:398–405.
[127] Campanari S. Thermodynamic model and parametric analysis of a tubular SOFC module. Journal of Power Sources 2001;92:26–34.
[128] Colclasure AM, Sanandaji BM, Vincent TL, Kee Rj. Modeling and control of tubular solid-oxide fuel cell systems. I: Physical models and linear model reduction. Journal of Power Sources 2010;196:196–207.
[129] Andreassi L, Rubeo G, Ubertini S, Lunghi P, Bove R. Experimental and numerical analysis of a radial flow solid oxide fuel cell. International Journal of Hydrogen Energy 2007;32:4559–74.
[130] Hofmann P, Panopoulos KD, Fryda LE, Kakaras E. Comparison between two methane reforming models applied to a quasi-two-dimensional planar solid oxide fuel cell model. Energy 2009;34:2151–7.
[131] Li P, Chyu M. Electrochemical and transport phenomena in solid oxide fuel cells. Heat Transfer Transactions ASME 2005;127:1344–62.
[132] Ho TX, Kosinski P, Hoffmann AC, Vik A. Effects of heat sources on the performance of a planar solid oxide fuel cell. International Journal of Hydrogen Energy 2010;35:4276–84.
[133] Khaleel MA, Lin Z, Singh P, Surdoval W, Collin D. A finite element analysis modeling tool for solid oxide fuel cell development: coupled electrochemistry, thermal and flow analysis in MARC®. Journal of Power Sources 2004;130:136–48.
[134] Ni M. Modeling of a solid oxide electrolysis cell for carbon dioxide electrolysis. Chemical Engineering Journal 2010;164:246–54.
[135] Tang Y, Liu J. Effect of anode and Boudouard reaction catalysts on the performance of direct carbon solid oxide fuel cells. International Journal of Hydrogen Energy 2010;35:11188–93.
[136] Hussain MM, Li X, Dincer I. Mathematical modeling of planar solid oxide fuel cells. Journal of Power Sources 2006;161:1012–22.
[137] Recknagle KP, Ryan EM, Koeppel BJ, Mahoney LA, Khaleel MA. Modeling of electrochemistry and steam-methane reforming performance for simulating pressurized solid oxide fuel cell stacks. Journal of Power Sources 2010;195:6637–44.
[138] Akhtar N, Decent SP, Kendall K. Numerical modelling of methane-powered micro-tubular, single-chamber solid oxide fuel cell. Journal of Power Sources 2010;195:7796–807.
[139] Fuel Cell Handbook. EG&G Services, Parsons, Inc, Sciences Applications International Corporation; October 2000.
[140] Petruzzi L, Cocchi S, Fineschi F. A global thermo-electrochemical model for SOFC systems design and engineering. Journal of Power Sources 2003;118:96–107.
[141] Minh NQ, Takahashi T. Science and technology of ceramic fuel cells. Amsterdam: Elsevier; 1995.
[142] Neophytides SG. The reversed flow operation of a crossflow solid oxide fuel cell monolith. Chemical Engineering Science 1999;54:4603–13.
[143] Lazzaretto A, Toffolo A. Energy, economy and environment as objectives in multi-criterion optimization of thermal systems design. Energy 2004;29:1139–57.
[144] Larminie J, Dicks A. Fuel cell systems explained. 3rd ed. Chichester, West Sussex: John Wiley & Sons Inc.; 2003.
[145] Sleiti AK. Performance of tubular Solid Oxide Fuel Cell at reduced temperature and cathode porosity. Journal of Power Sources 2010;195:5719–25.
[146] Hirano A, Suzuki M, Ippommatsu M. Evaluation of a new solid oxide fuel cell system by nonisothermal modelling. Journal of Electrochemical Society 1992;139:2744–51.
[147] Kapadia S, Anderson WK. Sensitivity analysis for solid oxide fuel cells using a three-dimensional numerical model. Journal of Power Sources 2009;189:1074–82.
[148] Jiang W, Fang R, Khan JA, Dougal RA. Parameter setting and analysis of a dynamic tubular SOFC model. Journal of Power Sources 2006;162: 316–26.
[149] Jurado F. A method for the identification of solid oxide fuel cells using a Hammerstein model. Journal of Power Sources 2006;154:145–52.
[150] Sánchez D, Chacartegui R, Muñoz A, Sánchez T. Thermal and electrochemical model of internal reforming solid oxide fuel cells with tubular geometry. Journal of Power Sources 2006;160:1074–87.
[151] Murshed AM, Huang B, Nandakumar K. Estimation and control of solid oxide fuel cell system. Computers & Chemical Engineering 2010;34:96–111.
[152] Tanaka T, Inui Y, Urata A, Kanno T. Three dimensional analysis of planar solid oxide fuel cell stack considering radiation. Energy Conversion and Management 2007;48:1491–8.
[153] Padullés J, Ault GW, Mcdonald JR. An integrated SOFC plant dynamic model for power systems simulation. Journal of Power Sources 2000;86: 495–500.
[154] Tanner CW, Virkar AV. A simple model for interconnect design of planar solid oxide fuel cells. Journal of Power Sources 2003;113:44–56.
[155] Daun KJ, Beale SB, Liu F, Smallwood GJ. Radiation heat transfer in planar SOFC electrolytes. Journal of Power Sources 2006;157:302–10.
[156] Zhang X, Li G, Li J, Feng Z. Numerical study on electric characteristics of solid oxide fuel cells. Energy Conversion and Management 2007;48:977–89.
[157] Janardhanan VM, Deutschmann O. CFD analysis of a solid oxide fuel cell with internal reforming: coupled interactions of transport, heterogeneous catalysis and electrochemical processes. Journal of Power Sources 2006;162:1192–202.
[158] Fardadi M, Mueller F, Jabbari F. Feedback control of solid oxide fuel cell spatial temperature variation. Journal of Power Sources 2010;195:4222–33.
[159] Damm DL, Fedorov AG. Spectral radiative heat transfer analysis of the planar SOFC. Fuel Cell Science and Technology 2005;2:258–62.
[160] Ho TX, Kosinski P, Hoffmann AC, Vik A. Transport, chemical and electrochemical processes in a planar solid oxide fuel cell: Detailed three-dimensional modeling. Journal of Power Sources 2010;195:6764–73.
[161] Ahmed K, Foger K. Kinetics of internal steam reforming of methane on Ni/YSZ-based anodes for solid oxide fuel cells. Catalysis Today 2000;63:479–87.
[162] Vernoux P, Guillodo M, Fouletier J, Hammou A. Alternative anode material for gradual methane reforming in solid oxide fuel cells. Solid State Ionics 2000;135:425–31.
[163] Liu M, Wei G, Luo J, Sanger AR, Chuang KT. Use of metal sulfides as anode catalysts in H_2S.air SOFCs. Journal of Electrochemical Society 2003;150:1025–9.
[164] Slavov SV, Chuang KT, Sanger AR, Donini JC, Kot J, Petrovic S. A proton-conducting solid state H_2S–O_2 fuel cell. 1. Anode catalysts, and operation at atmospheric pressure and 20–90 °C. International Journal of Hydrogen Energy 1998;23:1203–12.
[165] Hadvig S. Gas emissivity and absorptivity—a thermodynamic study. Journal of the Institute of Fuel 1970;53:129–35.
[166] Incropera F, Dewitt D. Fundamentals of heat and mass transfer. 4th ed. New York: Wiley; 1996.
[167] Ota T, Koyama M, Wen C-J, Yamada K, Takahashi H. Object-based modeling of SOFC system: dynamic behavior of micro-tube SOFC. Journal of Power Sources 2003;118:430–9.
[168] Yuan J, Rokni M, Sundén B. Three-dimensional computational analysis of gas and heat transport phenomena in ducts relevant for anode-supported solid oxide fuel cells. International Journal of Heat and Mass Transfer 2003;46:809–21.
[169] Fryda L, Panopoulos KD, Kakaras E. Integrated CHP with autothermal biomass gasification and SOFC-MGT. Energy Conversion and Management 2008;49:281–90.
[170] Colpan CO, Dincer I, Hamdullahpur F. Thermodynamic modeling of direct internal reforming solid oxide fuel cells operating with syngas. International Journal of Hydrogen Energy 2007;32:787–95.

[171] Omosun AO, Bauen A, Brandon NP, Adjiman CS, Hart D. Modelling system efficiencies and costs of two biomass-fuelled SOFC systems. Journal of Power Sources 2004;131:96–106.
[172] Panopoulos KD, Fryda LE, Karl J, Poulou S, Kakaras E. High temperature solid oxide fuel cell integrated with novel allothermal biomass gasification: Part I: Modelling and feasibility study. Journal of Power Sources 2006;159:570–85.
[173] Cordiner S, Feola M, Mulone V, Romanelli F. Analysis of a SOFC energy generation system fuelled with biomass reformate. Applied Thermal Engineering 2007;27:738–47.
[174] Van Herle J, Maréchal F, Leuenberger S, Membrez Y, Bucheli O, Favrat D. Process flow model of solid oxide fuel cell system supplied with sewage biogas. Journal of Power Sources 2004;131:127–41.
[175] Van Herle J, Maréchal F, Leuenberger S, Favrat D. Energy balance model of a SOFC cogenerator operated with biogas. Journal of Power Sources 2003;118:375–83.
[176] Vasileiadis S, Ziaka-Vasileiadou Z. Biomass reforming process for integrated solid oxide-fuel cell power generation. Chemical Engineering Science 2004;59:4853–9.
[177] Baron S, Brandon N, Atkinson A, Steele B, Rudkin R. The impact of wood-derived gasification gases on Ni-CGO anodes in intermediate temperature solid oxide fuel cells. Journal of Power Sources 2004;126:58–66.
[178] Kaneko T, Brouwer J, Samuelsen GS. Power and temperature control of fluctuating biomass gas fueled solid oxide fuel cell and micro gas turbine hybrid system. Journal of Power Sources 2006;160:316–25.
[179] Staniforth J, Kendall K. Biogas powering a small tubular solid oxide fuel cell. Journal of Power Sources 1998;71:275–7.
[180] Pujare NU, Semkow KW, Sammells AF. A direct H_2S/air solid oxide fuel cell. Electrochemical Society 1987;134:2639–40.
[181] Aguilar L, Zha S, Cheng Z, Winnick J, Liu M. A solid oxide fuel cell operating on hydrogen sulfide (H_2S) and sulfur-containing fuels. Journal of Power Sources 2004;135:17–24.
[182] Wei G-L, Luo J-L, Sanger AR, Chuang KT, Zhong L. Li_2SO_4-based proton-conducting membrane for H_2S-air fuel cell. Journal of Power Sources 2005;145:1–9.
[183] Yates C, Winnick J. Anode materials for a hydrogen sulfide solid oxide fuel cell. Journal of Electrochemical Society 1999;146:2841–4.
[184] Liu M, He P, Luo JL, Sanger AR, Chuang KT. Performance of a solid oxide fuel cell utilizing hydrogen sulfide as fuel. Journal of Power Sources 2001;94:20–5.
[185] Chuang KT, Sanger AR, Slavov SV, Donini JC. A proton-conducting solid state H_2S-O_2 fuel cell. 3. Operation using H_2S-hydrocarbon mixtures as anode feed. International Journal of Hydrogen Energy 2001;26:103–8.
[186] Ni M. Computational fluid dynamics modeling of a solid oxide electrolyzer cell for hydrogen production. International Journal of Hydrogen Energy 2009;34:7795–806.
[187] Brett DJL, et al. Concept and system design for a ZEBRA battery-intermediate temperature solid oxide fuel cell hybrid vehicle. Journal of Power Sources 2006;157:782–98.
[188] Arpornwichanop A, Chalermpanchai N, Patcharavorachot Y, Assabumrungrat S, Tade M. Performance of an anode-supported solid oxide fuel cell with direct-internal reforming of ethanol. International Journal of Hydrogen Energy 2009;34:7780–8.
[189] Entchev E, Yang L. Application of adaptive neuro-fuzzy inference system techniques and artificial neural networks to predict solid oxide fuel cell performance in residential microgeneration installation. Journal of Power Sources 2007;170:122–9.
[190] Milewski J, Swirski K. Modelling the SOFC behaviours by artificial neural network. International Journal of Hydrogen Energy 2009;34:5546–53.
[191] Huo H-B, Zhong Z-D, Zhu X-J, Tu H-Y. Nonlinear dynamic modeling for a SOFC stack by using a Hammerstein model. Journal of Power Sources 2008;175:441–6.
[192] Wu X-J, Zhu X-J, Cao G-Y, Tu H-Y. Modeling a SOFC stack based on GA-RBF neural networks identification. Journal of Power Sources 2007;167:145–50.
[193] Wu X-J, Zhu X-J, Cao G-Y, Tu H-Y. Nonlinear modeling of a SOFC stack based on ANFIS identification. Simulation Modelling Practice and Theory 2008;16:399–409.
[194] Wu X-J, Zhu X-J, Cao G-Y, Tu H-Y. Dynamic modeling of SOFC based on a T-S fuzzy model. Simulation Modelling Practice and Theory 2008;16:494–504.
[195] Arriagada J, Olausson P, Selimovic A. Artificial neural network simulator for SOFC performance prediction. Journal of Power Sources 2002;112:54–60.
[196] Yang J, Li X, Mou H-G, Jian L. Control-oriented thermal management of solid oxide fuel cells based on a modified Takagi-Sugeno fuzzy model. Journal of Power Sources 2009;188:475–82.
[197] Wu X-J, Zhu X-J, Cao G-Y, Tu H-Y. Nonlinear modelling of a SOFC stack by improved neural networks identification. Journal of Zhejiang University 2007;8:1505–9.
[198] Huo H-B, Zhu X-J, Cao G-Y. Nonlinear modeling of a SOFC stack based on a least squares support vector machine. Journal of Power Sources 2006;162:1220–5.